Cell Metabolism

Isolation of extracellular fluids reveals novel secreted bioactive proteins from muscle and fat tissues

Graphical abstract

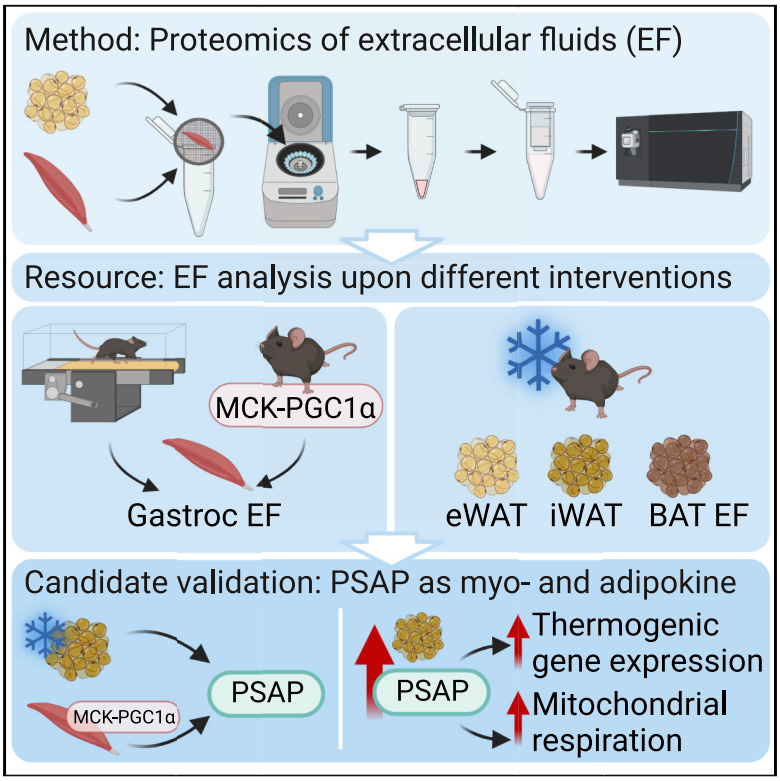

Authors

Melanie J. Mittenbühler, Mark P. Jedrychowski, Jonathan G. Van Vranken, ..., Steven P. Gygi, Edward T. Chouchani, Bruce M. Spiegelman

Correspondence

bruce_spiegelman@dfci.harvard.edu

In brief

Mittenbühler et al. developed a proteomics method for rapidly isolated extracellular fluid to identify novel secreted proteins from muscle and fat. Proteome profiling of these extracellular fluids reveals previously unknown secreted proteins in exercise, Pgc1α expression, and cold exposure and allows for high protein coverage compared with plasma proteomics.

Highlights

- Development of rapid EF isolation method for proteomics
- Quantification of previously unknown secreted proteins in EF of muscle and fat
- Resource of EF proteome changes in exercise, Pgc1α expression, and cold adaptation
- Identification of prosaposin as novel myokine and adipokine

Mittenbühler et al., 2023, Cell Metabolism *35*, 1–15
February 7, 2023 © 2022 Elsevier Inc.
https://doi.org/10.1016/j.cmet.2022.12.014

CellPress

Please cite this article in press as: Mittenbühler et al., Isolation of extracellular fluids reveals novel secreted bioactive proteins from muscle and fat tissues, Cell Metabolism (2022), https://doi.org/10.1016/j.cmet.2022.12.014

Cell Metabolism

CellPress

Resource

Isolation of extracellular fluids reveals novel secreted bioactive proteins from muscle and fat tissues

Melanie J. Mittenbühler,[1,2] Mark P. Jedrychowski,[1,2] Jonathan G. Van Vranken,[2] Hans-Georg Sprenger,[1,2] Sarah Wilensky,[1,2] Phillip A. Dumesic,[1,2] Yizhi Sun,[1,2] Andrea Tartaglia,[1,2] Dina Bogoslavski,[1] Mu A,[1,2] Haopeng Xiao,[1,2] Katherine A. Blackmore,[1,2] Anita Reddy,[1,2] Steven P. Gygi,[2] Edward T. Chouchani,[1,2] and Bruce M. Spiegelman[1,2,3,*]

[1]Department of Cancer Biology, Dana-Farber Cancer Institute, Boston, MA 02115, USA

[2]Department of Cell Biology, Harvard Medical School, Boston, MA 02115, USA

[3]Lead contact

*Correspondence: bruce_spiegelman@dfci.harvard.edu

https://doi.org/10.1016/j.cmet.2022.12.014

SUMMARY

Proteins are secreted from cells to send information to neighboring cells or distant tissues. Because of the highly integrated nature of energy balance systems, there has been particular interest in myokines and adipokines. These are challenging to study through proteomics because serum or plasma contains highly abundant proteins that limit the detection of proteins with lower abundance. We show here that extracellular fluid (EF) from muscle and fat tissues of mice shows a different protein composition than either serum or tissues. Mass spectrometry analyses of EFs from mice with physiological perturbations, like exercise or cold exposure, allowed the quantification of many potentially novel myokines and adipokines. Using this approach, we identify prosaposin as a secreted product of muscle and fat. Prosaposin expression stimulates thermogenic gene expression and induces mitochondrial respiration in primary fat cells. These studies together illustrate the utility of EF isolation as a discovery tool for adipokines and myokines.

INTRODUCTION

Proteins secreted from various tissues can mediate inter-organ crosstalk. These secreted factors can exert beneficial or detrimental effects, depending on their concentration, tissues, and context.[1,2] The secretome can be modulated by stimuli such as cold exposure and exercise.[3–5] Thus, identifying these potentially beneficial secreted proteins is of great interest. Although the computational analysis of transcriptomic or proteomic profiles from tissues may partially serve this purpose, this approach will likely miss many secreted proteins where the changes in secretion are not accompanied by changes at the mRNA levels and where the secretion/shedding is non-canonical. Serum or plasma proteomics analysis is a tool to identify novel secreted proteins from various different tissues potentially acting in an endocrine fashion.[6,7] However, despite the latest improvements in sample processing and instrument sensitivity, serum/plasma proteomics remains highly challenging. This can be attributed mainly to the tremendous variation in protein abundances, from mg/mL to pg/mL, the so-called dynamic range problem. In fact, the 12 most abundant proteins in serum and plasma account for approximately 95% of the total protein content, which often masks the detection of lower abundance proteins, such as hormones and cytokines.[8–10] Previous studies have developed techniques to increase mass spectrometry (MS) coverage on serum and plasma proteome by enriching for low abundance proteins through, for example, fractionation by two-dimensional gel electrophoresis,[11–13] immunoaffinity subtraction procedures,[14–16] protein enrichment technology,[17–19] or a combination of these methods. However, despite these efforts, the MS coverage remains low, and the discovery of potentially important molecules is either impossible or requires complex processing of initial samples, extensive MS instrument time, and/or genetic modifications.

Besides nutrients, extracellular fluid (EF) contains signaling molecules such as secreted proteins and metabolites. Local EF can be sampled through different techniques, e.g., the implantation of wicks,[20,21] micro-pipettes and catheters,[22] or capsules.[23] Another frequently used method for EF isolation is micro-dialysis, which has been used in various tissues.[24–27] Studies on skin EF have shown that 83% of proteins detected in serum can also be detected in the EF, whereas 50% of skin EF proteins cannot be detected in serum.[27–29] This suggests that the EF can serve as a source to identify novel extracellular and bioactive proteins. Here, we hypothesized that secreted proteins from tissues, as well as certain proteins coming from the circulation, can be detected via tissue EF proteomics and furthermore that EF profiling can provide a more comprehensive picture of extracellular proteins in the respective tissues. Although sampling EF can be performed using micro-dialysis

Please cite this article in press as: Mittenbühler et al., Isolation of extracellular fluids reveals novel secreted bioactive proteins from muscle and fat tissues, Cell Metabolism (2022), https://doi.org/10.1016/j.cmet.2022.12.014

and other methods,[25–27,30] an implantation requires surgical intervention, which itself can cause acute tissue trauma and induces an inflammatory response at the site of implantation.[24] In particular, the principle of micro-dialysis is based on passive diffusion of substances across a semipermeable membrane. This technique has been reported to suffer from macromolecular loss due to limited diffusion and recovery.[31] A previous study by Wiig and colleagues developed an elegant rapid EF isolation method using a low-speed centrifugation technique for tumor tissue.[32,33] This method has been utilized to study the extracellular metabolome in tumor and muscle tissues.[32,34–36] Moreover, this technique has been applied to analyze the proteome of EF from human ovarian carcinoma.[37] However, in-depth proteomic profiling of this rapidly isolated EF in muscle or adipose tissues has not been performed before. Here, we have developed a protocol to profile the EF proteome in response to different interventions in muscle and fat tissue, allowing for the discovery of previously unreported adipokines and myokines.

RESULTS

Muscle EF is distinct from muscle tissue and serum proteome and can serve as a potential discovery tool for secreted proteins in muscle tissue

To characterize the composition of EF, including potentially novel secreted proteins from muscle tissue, we adapted a previously developed technique for analyzing metabolites in the muscle EF.[32,34,36] Briefly, the gastrocnemius muscle—a muscle containing mixed fiber types—was dissected, the soleus was removed, and the muscle tissue was placed into a 20 μm mesh filter and centrifuged (600–800 g; Figure 1A). We first analyzed how the EF proteome differs qualitatively from that of muscle tissue, serum, and plasma by performing SDS-PAGE on these four different compartments (Figure S1A). These gels revealed that the protein pattern of muscle EF appeared distinct from muscle tissue, serum, and plasma. Although serum and plasma MS analyses remain highly challenging due to the extensive amount of highly abundant proteins, such as albumin and IGG, EF appeared to have reduced amounts of these proteins (Figure S1A). Nevertheless, albumin was still abundant in the EF of muscle (Figure S1B, asterisk). Therefore, we depleted the albumin from the EF to increase MS coverage using the R&D albumin/IGG immunodepletion resin, a kit intended to reduce the overwhelming abundance of these proteins in plasma and serum samples. As seen in Figure S1B, this resin effectively removed albumin from the EF samples and could potentially increase the polypeptide coverage of the MS analysis. We therefore incorporated this albumin depletion step in the preparation of all samples. Next, we determined EF volume/mass ratios for muscle (gastrocnemius) and also determined the protein concentration in muscle EF compared with plasma and serum (Figures S1C and S1D). As reported previously, the protein concentration of EF was lower than that of plasma or serum[33] (Figure S1D).

The protein content of the EF and the other biological compartments were compared by protein MS, using the tandem mass tag (TMT) method of isobaric labeling (Figures 1BI and 1BII; Tables S1 and S2). Principal component analysis of the two-by-two datasets demonstrated that when the EF was compared with either muscle tissue (Figures 1CI), or serum (Figures 1CII), there was a clear separation into distinct clusters. Gene Ontology (GO) analysis of upregulated proteins in EF versus muscle tissue (q value < 0.05) using the GOrilla program[38,39] further revealed that proteins associated with the extracellular space were upregulated in the EF compared with whole muscle tissue (Figure S1E) (cutoff enrichment > 1.5). Proteins associated with intracellular compartments were upregulated in muscle tissue (q value < 0.05) (Figure S1F) (cutoff enrichment > 1.5). The distinct EF proteome therefore likely represents the proteins enriched in a local compartment that is surrounding the myocytes.

We next analyzed the number of proteins annotated to be secreted by the UniProt dataset (SwissProt, subcellular location, downloaded January 2022[40]) across the EF and muscle tissue (Figure S1G). There were 856 proteins upregulated in EF when compared with muscle tissue (Figure 1D). Among these EF-upregulated proteins, 132 were annotated to be secreted, according to UniProt subcellular location. Thus, around 15.4% of EF-upregulated proteins were known to be secreted, whereas only 4.7% of muscle tissue upregulated proteins were annotated as secreted (Figure 1D). Furthermore, using Fisher's exact test, the power of the EF method to enrich for proteins annotated to be secreted was statistically significant (Figure 1E). Notably, proteins quantified in the EF, which were not annotated as secreted, may still be secreted through non-conventional pathways, and thus are not annotated as such in SwissProt. Thus, applying a filter for proteins annotated to be secreted will certainly cause the exclusion of interesting candidates.

Comparing proteins quantified in EF versus serum showed an upregulation of 833 proteins in EF, whereas only 324 proteins were upregulated in serum (Figure 1F). This suggests that we were indeed able to detect a more diverse protein composition in the EF. Of note, and as expected, a smaller proportion of proteins upregulated in EF was annotated as secreted when compared with serum proteins. This may reflect that the EF contains proteins that are secreted through various non-canonical secretion pathways, including extracellular vesicles, and also may reflect a certain amount of intracellular leakage. To further validate the extent of intracellular contamination in the EF centrifugate, we investigated whether highly abundant intracellular proteins are leaking into the EF during centrifugation. As seen in Figure S1H, commonly used marker proteins for cytosolic, ER, mitochondrial, Golgi, and nuclear proteins were greatly reduced in EF, suggesting rather minimal intracellular contamination of EF centrifugate. Whether the remaining signal for some markers stems from cell breakage or represents secretion through, for instance, the release of extracellular vesicles remains to be analyzed in the future.

Taken together, this newly established MS protocol shows that the EF method can enrich for secreted proteins and thereby allows for new discoveries. This approach can be used across many different genetic and environmental interventions.

Acute exercise training remodels the muscle EF proteome and impacts proteins of the coagulation and complement cascades

We next examined changes within the muscle EF proteome in response to a single, intense bout of exercise. A cohort of 8-week-old male C57BL/6J mice was assigned randomly to

Please cite this article in press as: Mittenbühler et al., Isolation of extracellular fluids reveals novel secreted bioactive proteins from muscle and fat tissues, Cell Metabolism (2022), https://doi.org/10.1016/j.cmet.2022.12.014

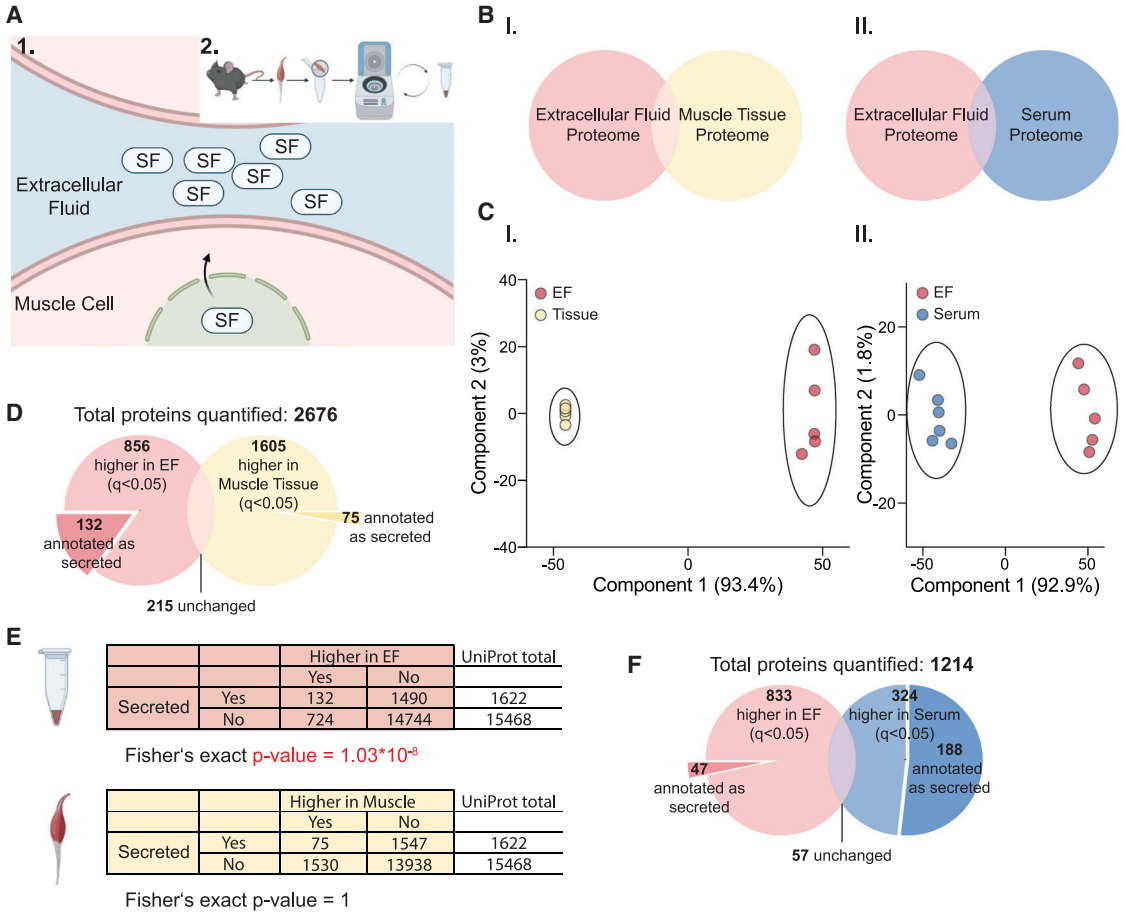

Figure 1. Muscle EF is distinct from muscle tissue and serum proteome and can serve as a potential discovery tool for secreted proteins in muscle tissue

(A) (1) Scheme of EF in the muscle tissue. SF, secreted factor. (2) Scheme of muscle EF isolation procedure.

(B) Scheme of MS experiment comparing (I) EF to muscle tissue and (II) EF to serum.

(C) Principal component analysis of (I) EF versus muscle tissue and (II) EF versus serum (n = 5–6 per compartment).

(D) Venn diagram of proteins increased in EF and muscle tissue. Proteins up/down determined by q value < 0.05.

(E) Fisher's exact test of secreted proteins in EF and muscle compared with the UniProt dataset.

(F) Venn diagram of proteins increased in EF and serum. Proteins up/down determined by q value < 0.05.

See also Figure S1 and Tables S1 and S2.

either an exercise or sedentary group. The exercise group was run vigorously on a treadmill for 45 min, with speeds ramped up as previously described (Figure 2A).[36] To get a measure of the amount of intracellular leakage into the EF samples, one pair of mice was injected intramuscularly with a GFP adenovirus and subjected to the exercise protocol. Subsequently, gastrocnemius muscle was harvested, EF was isolated, and tissue lysates were prepared. Western blot analysis showed no detectable GFP in the EF samples, even after this vigorous bout of exercise (Figure 2B). Furthermore, we performed a western blot analysis for commonly used, highly abundant, intracellular marker proteins and again did not observe leakage of these proteins into the EF, even after exercise (Figure 2C).

For proteomics analysis, we chose to isolate EF 60 min after an acute exercise bout, based on delayed *Ppargc1a* expression post-exercise in the gastrocnemius muscle. As shown in Figure S2A, muscle *Ppargc1a* gene expression increased after 30 min post-exercise and peaked around 60 min. In addition, serum interleukin (IL)-6 was significantly elevated 60 min post-exercise when compared with pre-exercise levels of the same mouse (Figure S2B). IL-6 is a well-known myokine induced and secreted with exercise.[41–44] Thus, IL-6 served as a positive control in the EF after acute exercise. As expected, elevated IL-6 levels were measured in EF isolated from exercised mice compared with sedentary control mice (Figure 2D).

The gastrocnemius muscle EF proteome was then analyzed from sedentary and exercised mice (Table S3). In total, we were able to quantify 6,507 proteins within the EF (Figure 2E).

To further filter the quantified proteins for secreted factors, we mapped the EF dataset onto the publicly available whole-protein classification database from UniProt, SwissProt as described in Figure S1G.[40] Among the 1,322 proteins that were significantly changed (q value < 0.05) in the EF of exercised versus sedentary mice, we quantified 40 upregulated and 35 downregulated

Please cite this article in press as: Mittenbühler et al., Isolation of extracellular fluids reveals novel secreted bioactive proteins from muscle and fat tissues, Cell Metabolism (2022), https://doi.org/10.1016/j.cmet.2022.12.014

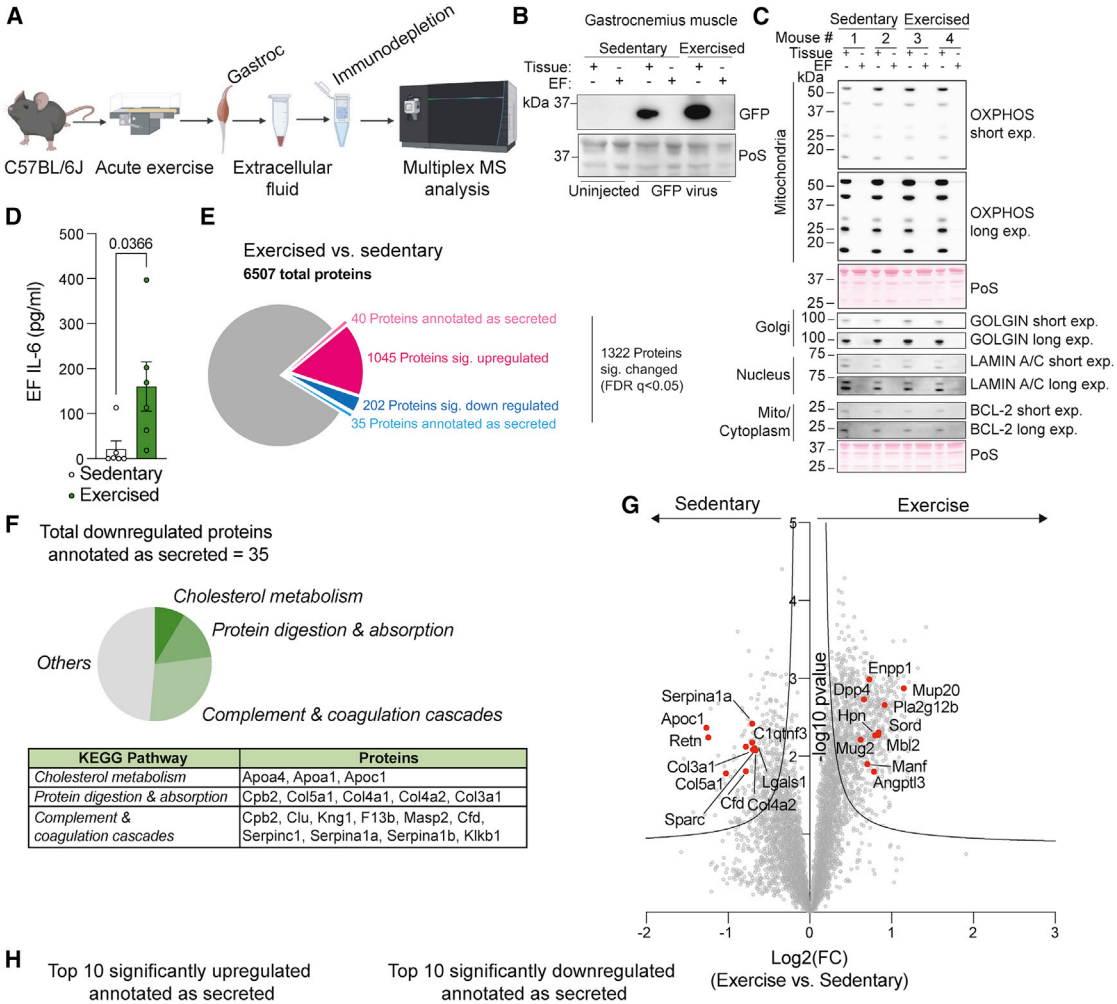

KEGG Pathway	Proteins
Cholesterol metabolism	Apoa4, Apoa1, Apoc1
Protein digestion & absorption	Cpb2, Col5a1, Col4a1, Col4a2, Col3a1
Complement & coagulation cascades	Cpb2, Clu, Kng1, F13b, Masp2, Cfd, Serpinc1, Serpina1a, Serpina1b, Klkb1

Figure 2. Acute exercise training remodels the muscle EF proteome and impacts proteins of the coagulation and complement cascades

(A) Scheme of acute exercise and EF isolation procedure and processing.

(B) Western blot of GFP protein expression in muscle EF and tissue of sedentary and exercised mice 2 weeks post-GFP adenovirus intramuscular injection.

(C) Western blot analysis of common intracellular marker proteins in muscle EF and tissue of sedentary and exercised mice.

(D) ELISA of EF IL-6 levels in sedentary and exercised mice (two-tailed unpaired t test, n = 6).

(E) Venn diagram of quantified proteins and significantly changed proteins upon acute exercise regimen (significant if q value < 0.05, n = 5–6 per group).

(F) KEGG pathway analysis of significantly downregulated proteins annotated as secreted in exercise. Gene symbols displayed.

(G) Volcano plot of top 10 upregulated and downregulated proteins annotated as secreted (significant if q value < 0.05, n = 5–6). Gene symbols displayed.

(H) Heatmap of top 10 upregulated and downregulated proteins annotated as secreted (q value < 0.05, n = 5–6). Data are presented as means ± SEM. Gene symbols displayed.

See also Figure S2 and Tables S3 and S4.

known secreted factors according to the UniProt database (Figures 2E and S2C). Interestingly, among the significantly downregulated proteins in the EF of exercised mice, we quantified many proteins that were associated with the complement and coagulation cascades according to KEGG pathway analysis (Figures 2F and S2D).[45] This finding is consistent with a recent publication that identified significantly changed proteins of the complement and coagulation cascades when analyzing plasma proteomics from mice that were trained for 4 weeks.[46] Of note, some factors reduced in our acute exercise EF proteomics

Please cite this article in press as: Mittenbühler et al., Isolation of extracellular fluids reveals novel secreted bioactive proteins from muscle and fat tissues, Cell Metabolism (2022), https://doi.org/10.1016/j.cmet.2022.12.014

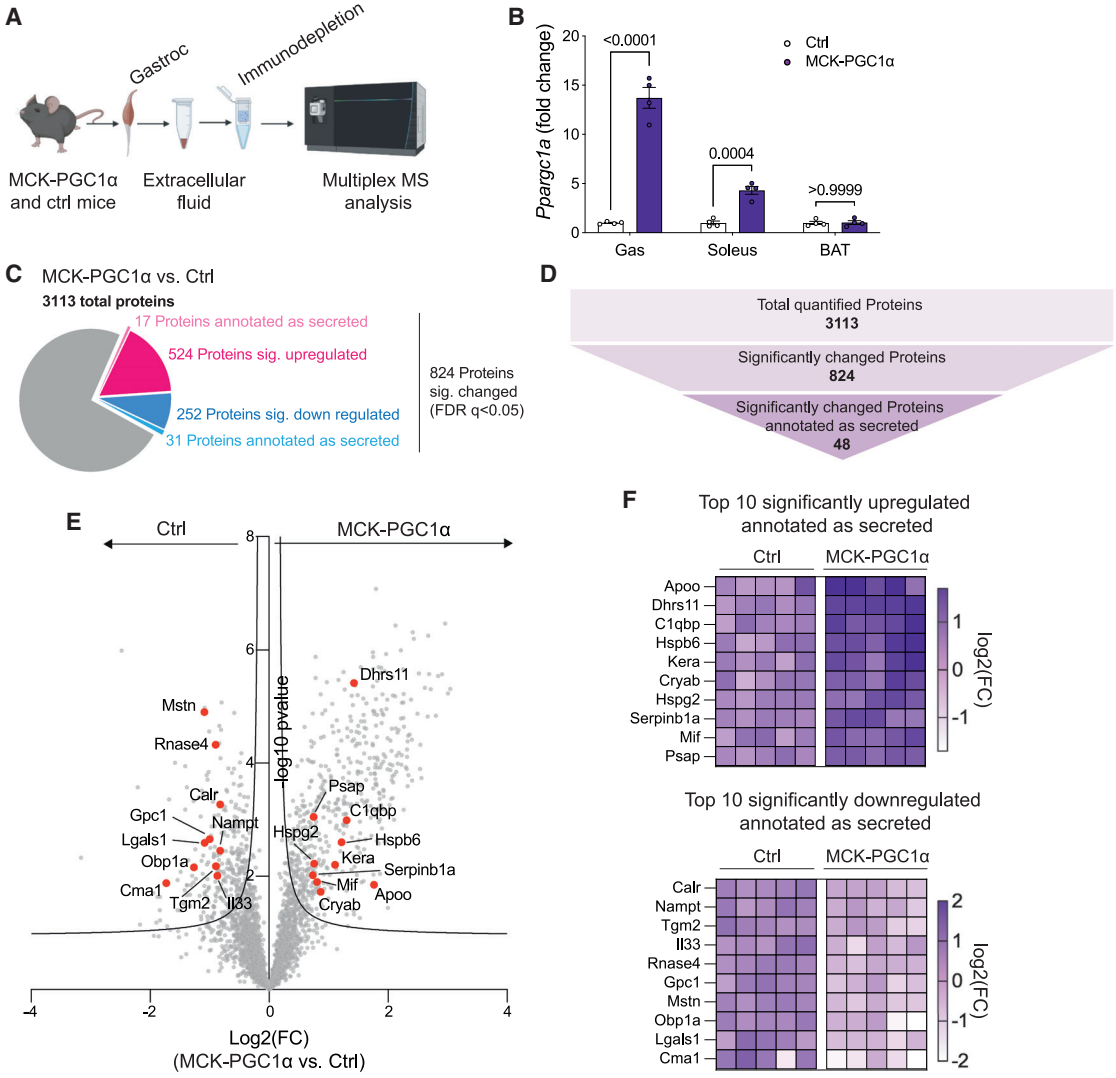

Figure 3. Muscle-specific PGC1α expression remodels EF proteome and reveals elevated protein levels of the neurotrophic factor prosaposin

(A) Scheme of MCK-PGC1α EF isolation procedure and processing.

(B) qRT-PCR of *Ppargc1a* gene expression normalized to *Rplp0* in different tissues (two-way ANOVA, n = 4). Gas, gastrocnemius muscle; BAT, brown adipose tissue.

(C) Venn diagram of quantified proteins and significantly changed proteins in MCK-PGC1α versus ctrl EF (significant if q value < 0.05, n = 5 per genotype).

(D) Scheme of data filtering procedure.

(E) Volcano plot of top 10 upregulated and downregulated proteins annotated as secreted (significant if q value < 0.05, n = 5). Gene symbols displayed.

(F) Heatmap of top 10 upregulated and downregulated proteins annotated as secreted (log_2 fold changes, n = 5). Data are presented as means ± SEM. Gene symbols displayed.

See also Figure S3 and Table S5.

were increased in plasma of these 4-week trained mice, including LIFR, CLU, QSOX1, F13B, MASP2, and KLKB1. This might be due to differences in exercise regimens and/or the difference in EF versus plasma proteome.

Importantly, the EF profiling also allowed for the quantification of secreted factors that have not been associated with exercise or muscle tissue before (Figures 2G and 2H). Among the top 10 upregulated candidates in exercise that were annotated to be secreted, phospholipase A2 group XIIB (PLA2G12B) and hepsin (HPN) were increased 1.8- and 1.7-fold, respectively. Both have been associated with high-density lipoprotein (HDL) levels in the blood.[47] Furthermore, sorbitol dehydrogenase (SORD) was increased 1.7-fold upon acute exercise. The loss of SORD function is related to slowly progressing hereditary motor axonopathy.[48] Thus, we provide a more comprehensive description of the EF proteome in the muscle tissue following an acute exercise protocol, including secreted proteins not previously associated with exercise and/or muscle tissue.

To examine reproducibility between preparations, we compared the sedentary control EF samples with an independently prepared

Please cite this article in press as: Mittenbühler et al., Isolation of extracellular fluids reveals novel secreted bioactive proteins from muscle and fat tissues, Cell Metabolism (2022), https://doi.org/10.1016/j.cmet.2022.12.014

TMT-plex of another cohort of sedentary mice (Table S4). Between these two independently run and prepared TMT-plexes, 89.4% and 74.7% of the total quantified proteins were identical in TMT-plex-1 and TMT-plex-2, respectively (Figure S2E). Then 5,819 proteins quantified in both TMT-plexes were rank-ordered, and the Spearman's coefficient was calculated (Figures S2E and S2F). The coefficient describes the correlation of the abundance order, of each commonly identified protein, in the two TMT-plexes. Importantly, proteins detected in both experiments had a very highly significant rank correlation across the two plexes of r_s = 0.8 and $p < 0.0001$, indicating a high reproducibility across these independent EF preparations.

Muscle-specific PGC1α expression remodels EF proteome and reveals elevated protein levels of the neurotrophic factor PSAP

Muscle-specific transgenic expression of PGC1α (MCK-PGC1α mice) has been proven to be a very useful genetic model, which mimics certain aspects of exercise, including angiogenesis and the stimulation of greater muscle innervation.[49–55] Forced expression of PGC1α is also sufficient to induce a fiber-type switch toward more oxidative fibers, as does endurance training.[49] The fiber-type phenotype in the MCK-PGC1α mice is present to a far greater extent than has been observed in trained mice or humans. Thus, the EF of MCK-PGC1α mice might provide a genetic tool for the identification of novel myokines, which are not present at detectable levels in models exercised within normal parameters. The EF of 8-week-old transgenic mice and their littermate controls were isolated, immunodepleted, and analyzed using MS (Figure 3A). MCK-PGC1α transgenic mice display a muscle-specific increase in *Ppargc1a* gene expression but not in other tissues, such as in brown adipose tissue (BAT) (Figure 3B). Proteomic analysis using the EF of MCK-PGC1α mice and their littermate controls quantified 3,113 proteins, among which 824 proteins were significantly changed between these groups (q value < 0.05) (Figures 3C and 3D; Table S5). Filtering for secreted proteins, we found 17 known secreted proteins to be upregulated, whereas 31 were downregulated. In line with previously published data, myostatin (MSTN) was among the top significantly downregulated proteins in the EF of MCK-PGC1α transgenic mice (Figures 3E and 3F).[56] Another very interesting candidate among the top 10 downregulated proteins in EF of MCK-PGC1α mice was nicotinamide phosphoribosyltransferase (NAMPT), whose extracellular form, eNAMPT, was reported to be elevated upon acute and chronic inflammation, such as obesity and insulin resistance[57] (Figures 3E and 3F). Among other interesting candidates within the top 10 upregulated proteins in the EF of MCK-PGC1α mice (Figures 3E and 3F), was the highly conserved glycoprotein prosaposin (PSAP), this was increased 1.66-fold in the EF of MCK-PGC1α mice (Figure S3A). This protein has not been previously identified as a myokine or adipokine. PSAP is the precursor of four active saposins (saposin A-D). Saposins are lysosomal proteins that activate sphingolipid hydrolysis through lysosomal hydrolases.[58,59] However, full-length PSAP is found in many secretory fluids including the blood and cerebrospinal fluid (CSF) and, interestingly, has been shown to act as a neurotrophic factor by preventing neuronal degradation and axonal loss. It has also been shown to induce nerve regeneration.[60–65] Of note, in the MS analysis 8 peptides of PSAP were quantified, covering several regions across the PSAP molecule (Figure S3B). This suggests that the detected molecule is probably the full-length PSAP protein.

EF proteome analysis identifies many cold-induced, secreted factors in thermogenic adipose tissue, including PSAP

Activating BAT and increasing the browning of white adipose tissue (WAT) can increase whole-body energy expenditure[66]—this represents a potential approach to treat obesity and associated metabolic diseases. However, beyond the regulation of energy expenditure, adipose tissue also affects glucose and lipid metabolism, insulin sensitivity, and acts as an endocrine organ by secreting adipokines.[67–70] In particular, brown and beige adipocytes secrete beneficial adipokines such as PM20D1,[71] Slit2-C,[72] follistatin (FST),[73] Epdr1,[74] and FGF21.[75] However, a more comprehensive report of proteins released from thermogenic adipose tissues is still needed. Thus, we applied this EF proteomic method to explore proteins released from thermogenic fat in mice. Upon cold adaptation, thermogenic fat depots increase the expression of certain genes leading to increases in non-shivering thermogenesis. BAT and subcutaneous fat depots such as the inguinal WAT (iWAT) respond to cold exposure with vigorous thermogenesis, whereas visceral fat depots such as the epididymal WAT (eWAT) do not. To profile the cold-induced EF proteome of 2 thermogenic fat depots (BAT and iWAT) and one non-thermogenic fat depot (eWAT), we housed mice for 2 weeks at cold temperatures (4°C) and subsequently isolated the EF from BAT, iWAT, and eWAT (Figure 4A). The protein composition was first analyzed via SDS-PAGE. Similar to muscle EF, adipose EF protein composition was obviously different from whole adipose tissue lysates (Figure S4A). As previously demonstrated, 2 weeks of cold exposure induced the expression of thermogenic genes in thermogenic fat (BAT and iWAT) but not to the same extent in eWAT (Figures 4B, S4B, and S4C).

EF volume varied among the different depots, with higher percent volume to tissue masses in iWAT and BAT compared with eWAT (Figure S4D). Protein concentration was lowest in iWAT and highest in BAT (Figure S4E). To determine the purity of EF isolated from these adipose tissue depots, western blots were performed for common intracellular marker proteins (Figures S4F–S4H). Lamin A and C, two nuclear markers, were not detectable in EF of all depots, whereas some proteins of the respiratory chain were detectable among these fluids with the highest abundance in eWAT (Figures S4F–S4H). However, these OXPHOS protein levels were still very low in EFs compared with respective tissue lysates.

Performing proteomics on EF of adipose tissues quantified a total of 3,844 proteins among which 1,579 proteins were significantly changed (q value < 0.05) in cold-exposed iWAT compared with cold-exposed eWAT (Figure 4C; Table S6). Following filtering for significantly changed proteins that were annotated as secreted, 172 proteins were found to be higher, whereas 41 proteins were lower expressed in iWAT versus eWAT EF (Figure 4C). In order to further filter for proteins expressed in the fat cells themselves, we also combined this proteomics list with published translating ribosome affinity purification (TRAP)-seq RNA datasets.[76] Roh et al. utilized

Please cite this article in press as: Mittenbühler et al., Isolation of extracellular fluids reveals novel secreted bioactive proteins from muscle and fat tissues, Cell Metabolism (2022), https://doi.org/10.1016/j.cmet.2022.12.014

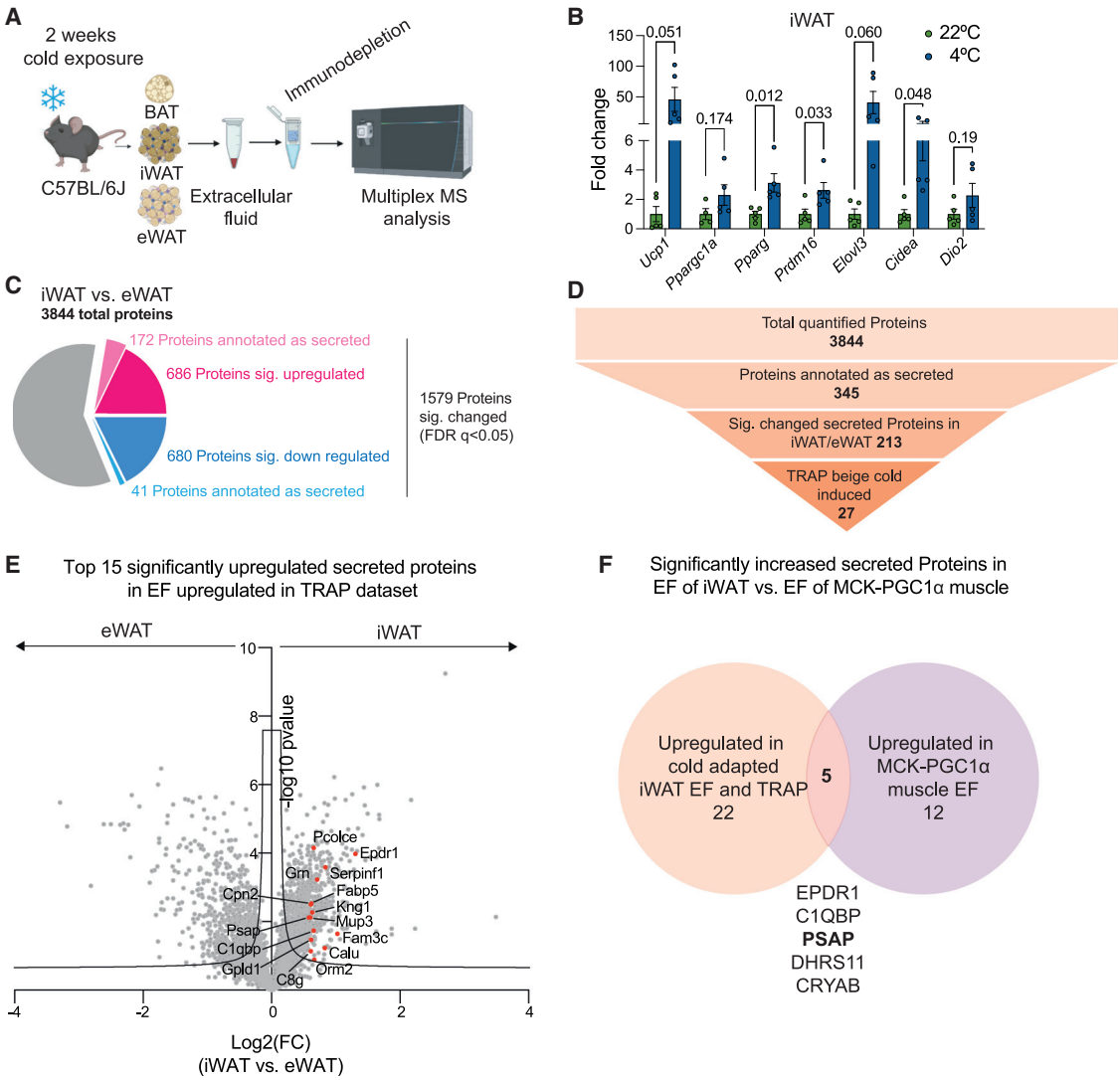

Figure 4. EF proteome analysis identifies many cold-induced, secreted factors in thermogenic adipose tissue, including PSAP

(A) Scheme of fat depot EF isolation procedure and processing.

(B) qRT-PCR of thermogenic gene expression normalized to *Rplp0* in iWAT after 2 weeks of room temperature or cold exposure (unpaired t test, n = 4–5).

(C) Venn diagram of quantified proteins and significantly changed proteins in cold-adapted EF of iWAT versus eWAT (significant if q value < 0.05, n = 4, EF pooled from 5 mice per sample).

(D) Scheme of data filtering procedure including overlay of upregulated proteins annotated as secreted in iWAT EF versus upregulated mRNA in TRAP dataset.[76]

(E) Volcano plot of top 15 upregulated proteins annotated as secreted in cold-adapted EF of iWAT versus eWAT (significant if q value < 0.05, n = 4, EF pooled from 5 mice per sample). Gene symbols displayed.

(F) Venn diagram of proteins annotated as secreted and significantly changed upon cold exposure in iWAT EF and PGC1α expression in muscle EF (significant if q value < 0.05). Data are presented as means ± SEM.

See also Figure S4 and Table S6.

Ucp1-NuTRAP (nuclear tagging and TRAP) mice and performed RNA sequencing (RNA-seq) to identify altered gene expression levels in warm versus cold-exposed beige adipocytes. Overlaying the secreted proteins that were significantly changed from our iWAT versus eWAT dataset with the TRAP-seq dataset revealed 27 commonly changed candidates (Figure 4D). Among these candidates, we identified known, cold-induced adipokines, such as EPDR1 (Figure 4E).[74] The browning of adipocytes requires elevated PGC1α levels to drive expression of the thermogenic gene program.[77] Consequently, we wanted to investigate whether there were common secreted proteins that were released upon forced PGC1α expression in the muscle-specific PGC1α transgenic mice and in cold exposed iWAT EF. To this end, we overlayed the MCK-PGC1α muscle EF dataset with the cold-induced iWAT EF dataset (Figure 4F). Among the significantly enriched secreted proteins, we found 5 proteins that were shared across the muscle and adipose EF, PSAP being one of them (Figure 4F). PSAP protein abundance was 1.5-fold higher in iWAT compared with eWAT EF (Figure S4I). Of note, the functions of PSAP in adipose tissue remain unexplored. Taken

Please cite this article in press as: Mittenbühler et al., Isolation of extracellular fluids reveals novel secreted bioactive proteins from muscle and fat tissues, Cell Metabolism (2022), https://doi.org/10.1016/j.cmet.2022.12.014

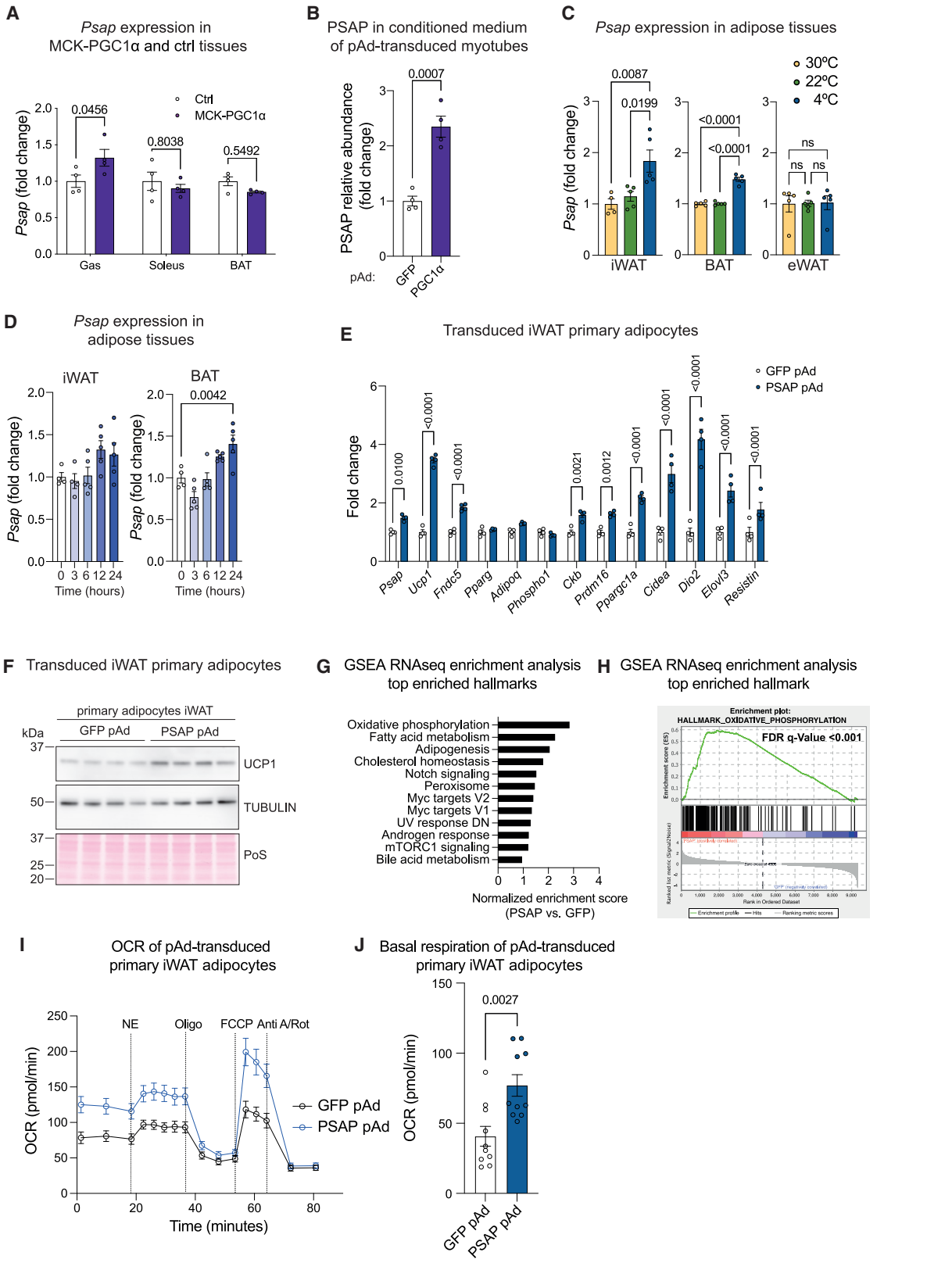

(legend on next page)

Please cite this article in press as: Mittenbühler et al., Isolation of extracellular fluids reveals novel secreted bioactive proteins from muscle and fat tissues, Cell Metabolism (2022), https://doi.org/10.1016/j.cmet.2022.12.014

CellPress

together, these data show that the EF from different fat depots contained previously unrecognized secreted factors that were induced upon cold exposure in thermogenic iWAT but not in non-thermogenic eWAT.

PSAP expression and secretion are induced by PGC1α and cold adaptation in muscle and fat, and PSAP expression is sufficient to boost oxidative metabolism in primary iWAT adipocytes

The identification of increased PSAP in EF from models involving the increased expression of PGC1α prompted us to study whether this gene is expressed in a PGC1α-dependent manner. Gene expression analysis of gastrocnemius muscle from MCK-PGC1α mice revealed a mild but significant induction of *Psap* expression when compared with their littermate controls (Figure 5A). However, in the soleus, forced PGC1α expression was not sufficient to induce *Psap* gene expression (Figure 5A), perhaps due to high PGC1α levels in the wild-type soleus muscle (Figure 3B). Next, we investigated whether muscle cells were able to secrete PSAP protein upon exogenous PGC1α expression. Primary myotubes were transduced with a PGC1α-expressing adenovirus or a GFP-expressing control adenovirus. Subsequently, proteins in the conditioned medium were determined via MS analysis (Table S7). The expression of PGC1α resulted in a significant, 2.3-fold increase of PSAP secretion into the medium (Figure 5B).

Psap gene expression was then examined in iWAT, BAT, and eWAT of mice housed at different temperatures. Mice were housed at 30°C (thermoneutrality), 22°C (room temperature), or 4°C for 2 weeks. *Psap* mRNA was specifically induced in thermogenic fat after 2 weeks of cold exposure, whereas non-thermogenic eWAT did not show this induction (Figure 5C). Subsequently, we investigated whether short-term cold exposure is sufficient to induce *Psap* expression in thermogenic fat depots. We found a mild increase of *Psap* levels after 12 h of cold exposure in BAT, whereas short-term cold exposure was not sufficient to significantly induce *Psap* expression in iWAT (Figure 5D).

As PSAP expression and secretion correlated with the cold-induced remodeling of thermogenic fat, we studied the effects of forced PSAP expression on the adipose cells. PSAP expression using a viral vector induced the expression of essential thermogenic genes, as well as brown adipocyte identity genes, such as *Prdm16*, *Cidea*, *Dio2*, and *Elovl3* (Figure 5E). Furthermore, the expression of PSAP resulted in higher UCP1 protein levels compared with cells transduced with the GFP control adenovirus (Figure 5F). To comprehensively profile transcriptional changes upon forced *Psap* expression, we performed RNA-seq analysis on pAd-PSAP or pAd-GFP transduced primary iWAT cells. Downstream gene set enrichment analysis (GSEA) [78,79] of hallmarkgene sets, which were increased upon *Psap* expression revealed oxidative phosphorylation as the top upregulated gene set (Figures 5G and 5H). In line with this evidence, forced expression of PSAP was sufficient to boost overall and basal respiration in iWAT cells (Figures 5I and 5J), thus suggesting that PSAP plays a previously unrecognized function in fat cell metabolism.

DISCUSSION

In this study, we developed a simple and rapid protocol for the analysis of the EF proteome. We show that this method can be adapted to different genetic and environmental interventions, such as exercise, tissue-specific transgenic expression of PGC1α, and cold exposure. It is also applicable to different tissues, like muscle and various adipose depots. Importantly, it is demonstrated that the composition and complexity of the EF proteome are distinct from that of serum and tissues. The EF proteomic method can presumably also be applied to many other tissues, including those of humans. This may lead to the development of new biomarkers, as well as provide potential new targets for therapeutic interventions.

Previously, several proximity biotinylation systems have been developed to identify secreted factors from specific tissues. The Finkel group developed an elegant mouse model, termed the secretome mouse, which conditionally expresses a proximal biotinylation system in the lumen of the endoplasmic reticulum (ER), resulting in the labeling of proteins that are secreted through the conventional secretory pathway.[80] Secreted proteins in serum of these mice can be enriched by streptavidin

Figure 5. PSAP expression and secretion are induced by PGC1α and cold adaptation in muscle and fat and PSAP expression is sufficient to boost oxidative metabolism in primary iWAT adipocytes

(A) qRT-PCR of *Psap* gene expression normalized to *Rplp0* in different tissues of MCK-PGC1α mice (two-way ANOVA, n = 4). Gas, gastrocnemius muscle; BAT, brown adipose tissue.

(B) PSAP intensity in conditioned medium of PGC1α- and GFP-transduced primary myotubes (unpaired t test, n = 4).

(C) qRT-PCR of *Psap* gene expression normalized to *Rplp0* in different fat depots upon thermoneutrality (30°C), room temperature (22°C), or cold exposure (4°C) (one-way ANOVA, n = 4–5). iWAT, inguinal white adipose tissue; BAT, brown adipose tissue; eWAT, epididymal white adipose tissue.

(D) qRT-PCR of *Psap* gene expression in iWAT and BAT upon different times of cold exposure (one-way ANOVA, n = 4–5). iWAT, inguinal white adipose tissue; BAT, brown adipose tissue.

(E) qRT-PCR of thermogenic gene expression and brown-fat identity genes normalized to *Rplp0* in primary iWAT adipocytes transduced with GFP- or PSAP-adenovirus (pAd) (two-way ANOVA, n = 4).

(F) Western blot of UCP1 protein expression in primary iWAT adipocytes transduced with GFP- or PSAP-pAd (n = 4).

(G) Top upregulated hallmarks in GSEA enrichment analysis of RNA-seq data of primary iWAT adipocytes transduced with GFP- or PSAP-pAd.

(H) Enrichment plot of top upregulated hallmark oxidative phosphorylation in GSEA enrichment analysis of RNA-seq data from primary iWAT adipocytes transduced with GFP- or PSAP-pAd (q value < 0.001, n = 4).

(I) Oxygen consumption rate (OCR) of iWAT adipocytes transduced with GFP- or PSAP-pAd (n = 10). NE, norepinephrine; Oligo, oligomycin; FCCP, carbonilcyanide p-triflouromethoxyphenylhydrazone; Rot, rotenone; Anti A, antimycin A.

(J) Basal OCR of iWAT adipocytes transduced with PSAP or GFP adenovirus (two-tailed unpaired t test, n = 10). Data are presented as means ± SEM.

See also Table S7.

Please cite this article in press as: Mittenbühler et al., Isolation of extracellular fluids reveals novel secreted bioactive proteins from muscle and fat tissues, Cell Metabolism (2022), https://doi.org/10.1016/j.cmet.2022.12.014

purification. Although highly specific, this system requires time-consuming breeding, as well as high biotin plasma levels achieved through injections and biotin feeding.[80] To overcome the time-consuming breeding step of transgenic mice, a conditional adeno-associated virus expressing an ER biotin ligase has been developed, which can be injected locally to label secreted proteins from specific tissues.[81] However, whole-proteome profiling of EF, as done here, has several advantages over these approaches. The EF method is quick and simple and does not require any genetic manipulations, injections, or feeding of chemicals—all of these may interfere with disease processes or impact homeostasis.[82] Additionally, our EF proteomic workflow allows for the detection of proteins that do not use the conventional secretory pathway through the ER lumen.

Although the EF proteomics method already allows for identifying many secreted proteins, as illustrated here, it could be further broadened by adding a treatment step with glycosidases. This step could allow better MS detection of very heavily glycosylated proteins such as the myokine irisin. Many such heavily glycosylated proteins exist in plasma or serum.

Another limitation of our method might be the occurrence of some cell breakage during the isolation procedure and subsequent leakage of intracellular contents into the EF. Although this likely happens to a certain extent, we were unable to detect several highly abundant intracellular proteins (or GFP) in muscle EF. Additionally, another study using a similar rapid EF isolation failed to detect intracellular metabolite classes in the muscle EF.[36] This leakage problem is particularly important to consider for softer tissues, such as adipose tissue. There, some intracellular proteins from the respiratory chain were detected at low but significant levels. However, we again cannot rule out that these proteins are actively secreted by extracellular vesicles, as recently described,[83] or are due to cellular leakage during the isolation procedure. The application of a filtering procedure using the SwissProt subcellular location database can help here, at the potential cost of losing information concerning proteins secreted non-canonically. This has been done in this study and allows to exclude potential intracellular, non-secreted proteins in the EF.

Using this approach, we have been able to identify known myokines, such as IL-16, IL-18, and decorin (DCN), which can be difficult to detect in serum proteomics due to their relatively low concentrations.[46] Interestingly, in muscle EF, we did also detect bona fide hepatokines and adipokines, which are known to be regulated in response to exercise, such as FST, angiopoietin-like 4 (ANGPTL4), adiponectin (ADIPOQ), and resistin (RETN).[84]

Importantly, several novel polypeptides were found that might contribute to the beneficial effects of exercise, such as PLA2G12B, HPN, and SORD in acute exercise muscle EF. Loss of function of PLA2G12B and HPN have both been correlated with low serum HDL levels in a mutagenesis screen[47]; however, these have not been investigated in the context of exercise. Notably, favorable HDL increased with exercise and is believed to reduce the risk for cardiovascular diseases.[85] Thus, PLA2G12B and HPN are potential candidates in the regulation of increased HDL upon exercise. Another interesting candidate induced with acute exercise is SORD, an enzyme metabolizing sorbitol to fructose.[86,87] Recently, SORD deficiency has been linked to slowly progressing hereditary motor axonopathy caused by a mutation in the SORD gene.[48] Patients with SORD deficiency displayed 100 times higher sorbitol levels in the blood, suggesting that SORD deficiency drives sorbitol-induced nerve toxicity. To our knowledge, SORD has not been linked to exercise before and could serve as a potential beneficial factor to clear increased sorbitol levels from the blood.

NAMPT was among the top 10 downregulated proteins in the EF of MCK-PGC1α mice. Intracellular NAMPT regulates the nicotinamide adenine dinucleotide (NAD) pool by impacting the activity of NAD-dependent enzymes.[88,89] eNAMPT has been detected in mouse and human circulation[90,91] and is elevated under conditions of acute and chronic inflammation, such as obesity and insulin resistance.[57] However, the extracellular regulation and function of this enzyme are still debated. Reduced eNAMPT might be a potential link between physiologic conditions showing elevated PGC1α expression and changes in insulin sensitivity.

Finally, because of the metabolic benefits brought by PGC1α in both muscle and fat tissues, we have long been interested in myokines and adipokines regulated by PGC1α.[92,93]

Here, we identify PSAP in the EF of iWAT upon cold adaptation and in muscle EF of MCK-PGC1α mice *in vivo*. Full-length PSAP, which is a precursor for the lysosomal proteins Saposins A–D, exerts neurotrophic functions in the central nervous system and periphery.[60–65] Of note, other neurotrophic factors, e.g., brain-derived neurotrophic factor (BDNF), have been shown to be secreted by contracting skeletal muscle and also play a role in adipose thermogenesis.[94,95] To date, PSAP expression has not been investigated in adipose tissues. As shown here, the forced expression of *Psap* exerts effects on the adipogenic gene program of adipocytes as well as on genes involved in oxidative phosphorylation. Interestingly, PSAP has been linked to organellar crosstalk between lysosomes and mitochondria.[96] Furthermore, the siRNA-mediated knockdown of *Psap* in murine bone marrow-derived macrophages reduces oxygen consumption rates (OCRs).[97] We show here that forced *Psap* expression was sufficient to boost OCRs in primary iWAT cells. Although unexplored here, PSAP could potentially play an important role in the elevated muscle innervation and neuromuscular junctions (NMJs) observed in MCK-PGC1α mice.[50,53] In fact, a previous study has shown that PSAP induces nerve regeneration after sciatic nerve injury[62]; however, its exact roles in muscle tissues remain to be determined.

Limitations of study

The EF proteomic analysis described in this study uses a centrifugation technique to isolate the EFs from different tissues. Although we have shown that the EF isolated through this technique seems to have only minimal contamination with intracellular "marker" proteins, we would like to highlight again that it is important to further validate potential secreted proteins via different approaches, as done here for PSAP. In addition, it should be considered that the EF most likely contains extracellular vesicles and their contents. It is also important to note that this method may miss candidates that are highly glycosylated or bound to albumin, as the protocol includes an albumin depletion step. If necessary, deglycosylation could be included in the sample preparation.

Please cite this article in press as: Mittenbühler et al., Isolation of extracellular fluids reveals novel secreted bioactive proteins from muscle and fat tissues, Cell Metabolism (2022), https://doi.org/10.1016/j.cmet.2022.12.014

STAR★METHODS

Detailed methods are provided in the online version of this paper and include the following:

- KEY RESOURCES TABLE
- RESOURCE AVAILABILITY
  - Lead contact
  - Materials availability
  - Data and code availability
- EXPERIMENTAL MODEL AND SUBJECT DETAILS
  - Mice
  - Cell culture
- METHOD DETAILS
  - Exercise protocol
  - Exposure to 4°C, 22°C, or 30°C
  - Extracellular fluid isolation
  - Immunodepletion of EF and Serum
  - Primary myoblast isolation and culturing
  - Conditioned medium preparation for mass spectrometry
  - Muscle Tissue preparation for Mass Spectrometry
  - Protein digest and peptide isobaric labeling
  - Mass spectrometry data acquisition
  - Mass spectrometry data analysis
  - Statistical analysis MS
  - IL-6 ELISA
  - Gene expression analysis by qRT-PCR
  - Primary adipocyte isolation and cell culture
  - Recombinant adenovirus preparation
  - Recombinant adenovirus transduction
  - Protein isolation
  - SDS-PAGE, Silver Stain, and Western Blot
  - Mitochondrial respiration
  - RNA sequencing
- QUANTIFICATION AND STATISTICAL ANALYSIS

SUPPLEMENTAL INFORMATION

Supplemental information can be found online at https://doi.org/10.1016/j.cmet.2022.12.014.

ACKNOWLEDGMENTS

The authors thank all members of the Spiegelman laboratory for valuable discussions and input. M.J.M. is funded by the Deutsche Forschungsgemeinschaft (DFG, German research foundation)—Projektnummer 461079553 and was funded by the NIH/NHLBI Training Program in Cardiovascular Research 5T32HL007374-41. J.G.V.V. is the Mark Foundation for Cancer Research Fellow of the Damon Runyon Cancer Research Foundation (DRG 2359-19). H.-G.S. is a Hope Funds for Cancer Research Fellow supported by the Hope Funds for Cancer Research (HFCR-20-03-01-02). Y.S. was supported by the American Heart Association postdoctoral fellowship. P.A.D. is supported by a Damon Runyon Cancer Research Foundation Fellowship (DRG 120-17). A.R. is supported by an F31 Predoctoral National Research Service Award from NIH, NIDDK. H.X. is supported by a K99 Award from the NIH (NIH K99AG073461). M.A. is supported by NIH F32 (1F32DK132864-01). Furthermore, the authors want to thank the DFCI Genomics Facility for RNA-seq analysis. This work was supported by the Claudia Adams Barr Program (E.T.C.), the Lavine Family Fund (E.T.C.), the Pew Charitable Trust (E.T.C.), NIH DK123095 (E.T.C.), the JPB Foundation 6293803 (B.M.S.), and NIH grants DK123228 and DK119117 (B.M.S.).

AUTHOR CONTRIBUTIONS

M.J.M. and B.M.S. designed the project and experiments and wrote the manuscript. M.P.J., M.J.M., and J.G.V.V. prepared samples for MS and performed data analysis. M.P.J. and J.G.V.V. performed MS analysis. M.J.M., S.W., A.T., H.-G.S., D.B., M.A., and K.A.B. performed and assisted with experiments. A.R. assisted with exercise experiments and EF isolation. P.A.D. performed primary myotube experiments. Y.S. assisted with cold exposure experiments. H.X., S.P.G., and E.T.C. contributed to data analysis and interpretation.

DECLARATION OF INTERESTS

B.M.S. holds patents related to irisin (WO2015051007A1). B.M.S. is an academic co-founder and consultant for Aevum Therapeutics. E.T.C. is a co-founder, equity holder, and board member of Matchpoint Therapeutics and a co-founder and equity holder in Aevum Therapeutics.

INCLUSION AND DIVERSITY

We support inclusive, diverse, and equitable conduct of research.

Received: June 8, 2022
Revised: October 24, 2022
Accepted: December 21, 2022
Published: January 20, 2023

REFERENCES

1. Severinsen, M.C.K., and Pedersen, B.K. (2020). Muscle-organ crosstalk: the emerging roles of myokines. Endocr. Rev. *41*, 594–609. https://doi.org/10.1210/endrev/bnaa016.
2. de Oliveira Dos Santos, A.R., de Oliveira Zanuso, B., Miola, V.F.B., Barbalho, S.M., Santos Bueno, P.C., Flato, U.A.P., Detregiachi, C.R.P., Buchaim, D.V., Buchaim, R.L., Tofano, R.J., et al. (2021). Adipokines, myokines, and hepatokines: crosstalk and metabolic repercussions. Int. J. Mol. Sci. *22*, 2639. https://doi.org/10.3390/ijms22052639.
3. Leuchtmann, A.B., Adak, V., Dilbaz, S., and Handschin, C. (2021). The role of the skeletal muscle secretome in mediating endurance and resistance training adaptations. Front. Physiol. *12*, 709807. https://doi.org/10.3389/fphys.2021.709807.
4. Villarroya, J., Cereijo, R., Gavaldà-Navarro, A., Peyrou, M., Giralt, M., and Villarroya, F. (2019). New insights into the secretory functions of brown adipose tissue. J. Endocrinol. *243*, R19–R27. https://doi.org/10.1530/JOE-19-0295.
5. Murphy, R.M., Watt, M.J., and Febbraio, M.A. (2020). Metabolic communication during exercise. Nat. Metab. *2*, 805–816. https://doi.org/10.1038/s42255-020-0258-x.
6. Geyer, P.E., Kulak, N.A., Pichler, G., Holdt, L.M., Teupser, D., and Mann, M. (2016). Plasma proteome profiling to assess human health and disease. Cell Syst. *2*, 185–195. https://doi.org/10.1016/j.cels.2016.02.015.
7. Geyer, P.E., Voytik, E., Treit, P.V., Doll, S., Kleinhempel, A., Niu, L., Müller, J.B., Buchholtz, M.L., Bader, J.M., Teupser, D., et al. (2019). Plasma proteome profiling to detect and avoid sample-related biases in biomarker studies. EMBO Mol. Med. *11*, e10427. https://doi.org/10.15252/emmm.201910427.
8. Anderson, N.L., and Anderson, N.G. (2002). The human plasma proteome: history, character, and diagnostic prospects. Mol. Cell. Proteomics *1*, 845–867. https://doi.org/10.1074/mcp.r200007-mcp200.
9. Hortin, G.L., Jortani, S.A., Ritchie, J.C., Jr., Valdes, R., Jr., and Chan, D.W. (2006). Proteomics: a new diagnostic frontier. Clin. Chem. *52*, 1218–1222. https://doi.org/10.1373/clinchem.2006.067280.
10. Hortin, G.L., Sviridov, D., and Anderson, N.L. (2008). High-abundance polypeptides of the human plasma proteome comprising the top 4 logs of polypeptide abundance. Clin. Chem. *54*, 1608–1616. https://doi.org/10.1373/clinchem.2008.108175.
11. Gygi, S.P., Corthals, G.L., Zhang, Y., Rochon, Y., and Aebersold, R. (2000). Evaluation of two-dimensional gel electrophoresis-based

Please cite this article in press as: Mittenbühler et al., Isolation of extracellular fluids reveals novel secreted bioactive proteins from muscle and fat tissues, Cell Metabolism (2022), https://doi.org/10.1016/j.cmet.2022.12.014

proteome analysis technology. Proc. Natl. Acad. Sci. USA *97*, 9390–9395. https://doi.org/10.1073/pnas.160270797.

12. Pieper, R., Gatlin, C.L., Makusky, A.J., Russo, P.S., Schatz, C.R., Miller, S.S., Su, Q., McGrath, A.M., Estock, M.A., Parmar, P.P., et al. (2003). The human serum proteome: display of nearly 3700 chromatographically separated protein spots on two-dimensional electrophoresis gels and identification of 325 distinct proteins. Proteomics *3*, 1345–1364. https://doi.org/10.1002/pmic.200300449.

13. Chromy, B.A., Gonzales, A.D., Perkins, J., Choi, M.W., Corzett, M.H., Chang, B.C., Corzett, C.H., and McCutchen-Maloney, S.L. (2004). Proteomic analysis of human serum by two-dimensional differential gel electrophoresis after depletion of high-abundant proteins. J. Proteome Res. *3*, 1120–1127. https://doi.org/10.1021/pr049921p.

14. Martosella, J., Zolotarjova, N., Liu, H., Nicol, G., and Boyes, B.E. (2005). Reversed-phase high-performance liquid chromatographic prefractionation of immunodepleted human serum proteins to enhance mass spectrometry identification of lower-abundant proteins. J. Proteome Res. *4*, 1522–1537. https://doi.org/10.1021/pr050088l.

15. Echan, L.A., Tang, H.Y., Ali-Khan, N., Lee, K., and Speicher, D.W. (2005). Depletion of multiple high-abundance proteins improves protein profiling capacities of human serum and plasma. Proteomics *5*, 3292–3303. https://doi.org/10.1002/pmic.200401228.

16. Pieper, R., Su, Q., Gatlin, C.L., Huang, S.T., Anderson, N.L., and Steiner, S. (2003). Multi-component immunoaffinity subtraction chromatography: an innovative step towards a comprehensive survey of the human plasma proteome. Proteomics *3*, 422–432. https://doi.org/10.1002/pmic.200390057.

17. Boschetti, E., and Righetti, P.G. (2008). The ProteoMiner in the proteomic arena: a non-depleting tool for discovering low-abundance species. J. Proteomics *71*, 255–264. https://doi.org/10.1016/j.jprot.2008.05.002.

18. Li, L. (2015). Dynamic range compression with ProteoMiner: principles and examples. Methods Mol. Biol. *1295*, 99–107. https://doi.org/10.1007/978-1-4939-2550-6_9.

19. Hartwig, S., Czibere, A., Kotzka, J., Passlack, W., Haas, R., Eckel, J., and Lehr, S. (2009). Combinatorial hexapeptide ligand libraries (ProteoMiner): an innovative fractionation tool for differential quantitative clinical proteomics. Arch. Physiol. Biochem. *115*, 155–160. https://doi.org/10.1080/13813450903154224.

20. Aukland, K., and Fadnes, H.O. (1973). Protein concentration of interstitial fluid collected from rat skin by a wick method. Acta Physiol. Scand. *88*, 350–358. https://doi.org/10.1111/j.1748-1716.1973.tb05459.x.

21. Fadnes, H.O., and Aukland, K. (1977). Protein concentration and colloid osmotic pressure of interstitial fluid collected by the wick technique: analysis and evaluation of the method. Microvasc. Res. *14*, 11–25. https://doi.org/10.1016/0026-2862(77)90137-6.

22. Haljamäe, H., and Fredén, H. (1970). Comparative analysis of the protein content of local subcutaneous tissue fluid and plasma. Microvasc. Res. *2*, 163–171. https://doi.org/10.1016/0026-2862(70)90004-x.

23. Guyton, A.C. (1963). A concept of negative interstitial pressure based on pressures in implanted perforated capsules. Circ. Res. *12*, 399–414. https://doi.org/10.1161/01.res.12.4.399.

24. Turkina, M.V., Ghafouri, N., Gerdle, B., and Ghafouri, B. (2017). Evaluation of dynamic changes in interstitial fluid proteome following microdialysis probe insertion trauma in trapezius muscle of healthy women. Sci. Rep. *7*, 43512. https://doi.org/10.1038/srep43512.

25. Ungerstedt, U. (1991). Microdialysis–principles and applications for studies in animals and man. J. Intern. Med. *230*, 365–373. https://doi.org/10.1111/j.1365-2796.1991.tb00459.x.

26. Ao, X., and Stenken, J.A. (2006). Microdialysis sampling of cytokines. Methods *38*, 331–341. https://doi.org/10.1016/j.ymeth.2005.11.012.

27. Samant, P.P., and Prausnitz, M.R. (2018). Mechanisms of sampling interstitial fluid from skin using a microneedle patch. Proc. Natl. Acad. Sci. USA *115*, 4583–4588. https://doi.org/10.1073/pnas.1716772115.

28. Kool, J., Reubsaet, L., Wesseldijk, F., Maravilha, R.T., Pinkse, M.W., D'Santos, C.S., van Hilten, J.J., Zijlstra, F.J., and Heck, A.J. (2007). Suction blister fluid as potential body fluid for biomarker proteins. Proteomics *7*, 3638–3650. https://doi.org/10.1002/pmic.200600938.

29. Müller, A.C., Breitwieser, F.P., Fischer, H., Schuster, C., Brandt, O., Colinge, J., Superti-Furga, G., Stingl, G., Elbe-Bürger, A., and Bennett, K.L. (2012). A comparative proteomic study of human skin suction blister fluid from healthy individuals using immunodepletion and iTRAQ labeling. J. Proteome Res. *11*, 3715–3727. https://doi.org/10.1021/pr3002035.

30. Lafontan, M., and Arner, P. (1996). Application of in situ microdialysis to measure metabolic and vascular responses in adipose tissue. Trends Pharmacol. Sci. *17*, 309–313.

31. Stenken, J.A., Church, M.K., Gill, C.A., and Clough, G.F. (2010). How minimally invasive is microdialysis sampling? A cautionary note for cytokine collection in human skin and other clinical studies. AAPS J. *12*, 73–78. https://doi.org/10.1208/s12248-009-9163-7.

32. Wiig, H., Aukland, K., and Tenstad, O. (2003). Isolation of interstitial fluid from rat mammary tumors by a centrifugation method. Am. J. Physiol. Heart Circ. Physiol. *284*, H416–H424. https://doi.org/10.1152/ajpheart.00327.2002.

33. Wiig, H., and Swartz, M.A. (2012). Interstitial fluid and lymph formation and transport: physiological regulation and roles in inflammation and cancer. Physiol. Rev. *92*, 1005–1060. https://doi.org/10.1152/physrev.00037.2011.

34. Spinelli, J.B., Yoon, H., Ringel, A.E., Jeanfavre, S., Clish, C.B., and Haigis, M.C. (2017). Metabolic recycling of ammonia via glutamate dehydrogenase supports breast cancer biomass. Science *358*, 941–946. https://doi.org/10.1126/science.aam9305.

35. Sullivan, M.R., Danai, L.V., Lewis, C.A., Chan, S.H., Gui, D.Y., Kunchok, T., Dennstedt, E.A., Vander Heiden, M.G., and Muir, A. (2019). Quantification of microenvironmental metabolites in murine cancers reveals determinants of tumor nutrient availability. eLife *8*, e44235. https://doi.org/10.7554/eLife.44235.

36. Reddy, A., Bozi, L.H.M., Yaghi, O.K., Mills, E.L., Xiao, H., Nicholson, H.E., Paschini, M., Paulo, J.A., Garrity, R., Laznik-Bogoslavski, D., et al. (2020). pH-gated succinate secretion regulates muscle remodeling in response to exercise. Cell *183*, 62–75.e17. https://doi.org/10.1016/j.cell.2020.08.039.

37. Haslene-Hox, H., Oveland, E., Berg, K.C., Kolmannskog, O., Woie, K., Salvesen, H.B., Tenstad, O., and Wiig, H. (2011). A new method for isolation of interstitial fluid from human solid tumors applied to proteomic analysis of ovarian carcinoma tissue. PLoS One *6*, e19217. https://doi.org/10.1371/journal.pone.0019217.

38. Eden, E., Lipson, D., Yogev, S., and Yakhini, Z. (2007). Discovering motifs in ranked lists of DNA sequences. PLoS Comput. Biol. *3*, e39. https://doi.org/10.1371/journal.pcbi.0030039.

39. Eden, E., Navon, R., Steinfeld, I., Lipson, D., and Yakhini, Z. (2009). GOrilla: a tool for discovery and visualization of enriched GO terms in ranked gene lists. BMC Bioinformatics *10*, 48. https://doi.org/10.1186/1471-2105-10-48.

40. UniProt Consortium (2021). UniProt: the universal protein knowledgebase in 2021. Nucleic Acids Res. *49*, D480–D489. https://doi.org/10.1093/nar/gkaa1100.

41. Ostrowski, K., Hermann, C., Bangash, A., Schjerling, P., Nielsen, J.N., and Pedersen, B.K. (1998). A trauma-like elevation of plasma cytokines in humans in response to treadmill running. J. Physiol. *513*, 889–894. https://doi.org/10.1111/j.1469-7793.1998.889ba.x.

42. Ostrowski, K., Rohde, T., Zacho, M., Asp, S., and Pedersen, B.K. (1998). Evidence that interleukin-6 is produced in human skeletal muscle during prolonged running. J. Physiol. *508*, 949–953. https://doi.org/10.1111/j.1469-7793.1998.949bp.x.

43. Pedersen, B.K. (2017). Anti-inflammatory effects of exercise: role in diabetes and cardiovascular disease. Eur. J. Clin. Investig. *47*, 600–611. https://doi.org/10.1111/eci.12781.

Please cite this article in press as: Mittenbühler et al., Isolation of extracellular fluids reveals novel secreted bioactive proteins from muscle and fat tissues, Cell Metabolism (2022), https://doi.org/10.1016/j.cmet.2022.12.014

44. Pedersen, B.K., and Febbraio, M.A. (2008). Muscle as an endocrine organ: focus on muscle-derived interleukin-6. Physiol. Rev. *88*, 1379–1406. https://doi.org/10.1152/physrev.90100.2007.

45. Szklarczyk, D., Franceschini, A., Wyder, S., Forslund, K., Heller, D., Huerta-Cepas, J., Simonovic, M., Roth, A., Santos, A., Tsafou, K.P., et al. (2015). STRING v10: protein-protein interaction networks, integrated over the tree of life. Nucleic Acids Res. *43*, D447–D452. https://doi.org/10.1093/nar/gku1003.

46. De Miguel, Z., Khoury, N., Betley, M.J., Lehallier, B., Willoughby, D., Olsson, N., Yang, A.C., Hahn, O., Lu, N., Vest, R.T., et al. (2021). Exercise plasma boosts memory and dampens brain inflammation via clusterin. Nature *600*, 494–499. https://doi.org/10.1038/s41586-021-04183-x.

47. Aljakna, A., Choi, S., Savage, H., Hageman Blair, R., Gu, T., Svenson, K.L., Churchill, G.A., Hibbs, M., and Korstanje, R. (2012). Pla2g12b and Hpn are genes identified by mouse ENU mutagenesis that affect HDL cholesterol. PLoS One *7*, e43139. https://doi.org/10.1371/journal.pone.0043139.

48. Cortese, A., Zhu, Y., Rebelo, A.P., Negri, S., Courel, S., Abreu, L., Bacon, C.J., Bai, Y., Bis-Brewer, D.M., Bugiardini, E., et al. (2020). Biallelic mutations in SORD cause a common and potentially treatable hereditary neuropathy with implications for diabetes. Nat. Genet. *52*, 473–481. https://doi.org/10.1038/s41588-020-0615-4.

49. Lin, J., Wu, H., Tarr, P.T., Zhang, C.Y., Wu, Z., Boss, O., Michael, L.F., Puigserver, P., Isotani, E., Olson, E.N., et al. (2002). Transcriptional co-activator PGC-1 alpha drives the formation of slow-twitch muscle fibres. Nature *418*, 797–801. https://doi.org/10.1038/nature00904.

50. Handschin, C., Kobayashi, Y.M., Chin, S., Seale, P., Campbell, K.P., and Spiegelman, B.M. (2007). PGC-1alpha regulates the neuromuscular junction program and ameliorates Duchenne muscular dystrophy. Genes Dev. *21*, 770–783. https://doi.org/10.1101/gad.1525107.

51. Sandri, M., Lin, J., Handschin, C., Yang, W., Arany, Z.P., Lecker, S.H., Goldberg, A.L., and Spiegelman, B.M. (2006). PGC-1alpha protects skeletal muscle from atrophy by suppressing FoxO3 action and atrophy-specific gene transcription. Proc. Natl. Acad. Sci. USA *103*, 16260–16265. https://doi.org/10.1073/pnas.0607795103.

52. Cannavino, J., Brocca, L., Sandri, M., Grassi, B., Bottinelli, R., and Pellegrino, M.A. (2015). The role of alterations in mitochondrial dynamics and PGC-1alpha over-expression in fast muscle atrophy following hindlimb unloading. J. Physiol. *593*, 1981–1995. https://doi.org/10.1113/jphysiol.2014.286740.

53. Chan, M.C., Rowe, G.C., Raghuram, S., Patten, I.S., Farrell, C., and Arany, Z. (2014). Post-natal induction of PGC-1alpha protects against severe muscle dystrophy independently of utrophin. Skelet. Muscle *4*, 2. https://doi.org/10.1186/2044-5040-4-2.

54. Garcia, S., Nissanka, N., Mareco, E.A., Rossi, S., Peralta, S., Diaz, F., Rotundo, R.L., Carvalho, R.F., and Moraes, C.T. (2018). Overexpression of PGC-1alpha in aging muscle enhances a subset of young-like molecular patterns. Aging Cell *17*, e12707. https://doi.org/10.1111/acel.12707.

55. Arany, Z., Foo, S.Y., Ma, Y., Ruas, J.L., Bommi-Reddy, A., Girnun, G., Cooper, M., Laznik, D., Chinsomboon, J., Rangwala, S.M., et al. (2008). HIF-independent regulation of VEGF and angiogenesis by the transcriptional coactivator PGC-1alpha. Nature *451*, 1008–1012. https://doi.org/10.1038/nature06613.

56. Dinulovic, I., Furrer, R., Di Fulvio, S., Ferry, A., Beer, M., and Handschin, C. (2016). PGC-1alpha modulates necrosis, inflammatory response, and fibrotic tissue formation in injured skeletal muscle. Skelet. Muscle *6*, 38. https://doi.org/10.1186/s13395-016-0110-x.

57. Chang, Y.H., Chang, D.M., Lin, K.C., Shin, S.J., and Lee, Y.J. (2011). Visfatin in overweight/obesity, type 2 diabetes mellitus, insulin resistance, metabolic syndrome and cardiovascular diseases: a meta-analysis and systemic review. Diabetes Metab. Res. Rev. *27*, 515–527. https://doi.org/10.1002/dmrr.1201.

58. Kishimoto, Y., Hiraiwa, M., and O'Brien, J.S. (1992). Saposins: structure, function, distribution, and molecular genetics. J. Lipid Res. *33*, 1255–1267.

59. O'Brien, J.S., and Kishimoto, Y. (1991). Saposin proteins: structure, function, and role in human lysosomal storage disorders. FASEB J. *5*, 301–308. https://doi.org/10.1096/fasebj.5.3.2001789.

60. Sano, A., Matsuda, S., Wen, T.C., Kotani, Y., Kondoh, K., Ueno, S., Kakimoto, Y., Yoshimura, H., and Sakanaka, M. (1994). Protection by prosaposin against ischemia-induced learning disability and neuronal loss. Biochem. Biophys. Res. Commun. *204*, 994–1000. https://doi.org/10.1006/bbrc.1994.2558.

61. O'Brien, J.S., Carson, G.S., Seo, H.C., Hiraiwa, M., and Kishimoto, Y. (1994). Identification of prosaposin as a neurotrophic factor. Proc. Natl. Acad. Sci. USA *91*, 9593–9596. https://doi.org/10.1073/pnas.91.20.9593.

62. Kotani, Y., Matsuda, S., Sakanaka, M., Kondoh, K., Ueno, S., and Sano, A. (1996). Prosaposin facilitates sciatic nerve regeneration in vivo. J. Neurochem. *66*, 2019–2025. https://doi.org/10.1046/j.1471-4159.1996.66052019.x.

63. Morita, F., Wen, T.C., Tanaka, J., Hata, R., Desaki, J., Sato, K., Nakata, K., Ma, Y.J., and Sakanaka, M. (2001). Protective effect of a prosaposin-derived, 18-mer peptide on slowly progressive neuronal degeneration after brief ischemia. J. Cereb. Blood Flow Metab. *21*, 1295–1302. https://doi.org/10.1097/00004647-200111000-00005.

64. Ochiai, T., Takenaka, Y., Kuramoto, Y., Kasuya, M., Fukuda, K., Kimura, M., Shimeno, H., Misasi, R., Hiraiwa, M., and Soeda, S. (2008). Molecular mechanism for neuro-protective effect of prosaposin against oxidative stress: its regulation of dimeric transcription factor formation. Biochim. Biophys. Acta *1780*, 1441–1447. https://doi.org/10.1016/j.bbagen.2008.07.010.

65. Gao, H.L., Li, C., Nabeka, H., Shimokawa, T., Saito, S., Wang, Z.Y., Cao, Y.M., and Matsuda, S. (2013). Attenuation of MPTP/MPP(+) toxicity in vivo and in vitro by an 18-mer peptide derived from prosaposin. Neuroscience *236*, 373–393. https://doi.org/10.1016/j.neuroscience.2013.01.007.

66. Cohen, P., and Spiegelman, B.M. (2016). Cell biology of fat storage. Mol. Biol. Cell *27*, 2523–2527. https://doi.org/10.1091/mbc.E15-10-0749.

67. Cohen, P., and Kajimura, S. (2021). The cellular and functional complexity of thermogenic fat. Nat. Rev. Mol. Cell Biol. *22*, 393–409. https://doi.org/10.1038/s41580-021-00350-0.

68. Fasshauer, M., and Blüher, M. (2015). Adipokines in health and disease. Trends Pharmacol. Sci. *36*, 461–470. https://doi.org/10.1016/j.tips.2015.04.014.

69. Cook, K.S., Min, H.Y., Johnson, D., Chaplinsky, R.J., Flier, J.S., Hunt, C.R., and Spiegelman, B.M. (1987). Adipsin: a circulating serine protease homolog secreted by adipose tissue and sciatic nerve. Science *237*, 402–405. https://doi.org/10.1126/science.3299705.

70. Zhang, Y., Proenca, R., Maffei, M., Barone, M., Leopold, L., and Friedman, J.M. (1994). Positional cloning of the mouse obese gene and its human homologue. Nature *372*, 425–432. https://doi.org/10.1038/372425a0.

71. Long, J.Z., Svensson, K.J., Bateman, L.A., Lin, H., Kamenecka, T., Lokurkar, I.A., Lou, J., Rao, R.R., Chang, M.R., Jedrychowski, M.P., et al. (2016). The secreted enzyme PM20D1 regulates lipidated amino acid uncouplers of mitochondria. Cell *166*, 424–435. https://doi.org/10.1016/j.cell.2016.05.071.

72. Svensson, K.J., Long, J.Z., Jedrychowski, M.P., Cohen, P., Lo, J.C., Serag, S., Kir, S., Shinoda, K., Tartaglia, J.A., Rao, R.R., et al. (2016). A secreted Slit2 fragment regulates adipose tissue thermogenesis and metabolic function. Cell Metab. *23*, 454–466. https://doi.org/10.1016/j.cmet.2016.01.008.

73. Singh, R., Braga, M., Reddy, S.T., Lee, S.J., Parveen, M., Grijalva, V., Vergnes, L., and Pervin, S. (2017). Follistatin targets distinct pathways to promote brown adipocyte characteristics in brown and white adipose

Please cite this article in press as: Mittenbühler et al., Isolation of extracellular fluids reveals novel secreted bioactive proteins from muscle and fat tissues, Cell Metabolism (2022), https://doi.org/10.1016/j.cmet.2022.12.014

tissues. Endocrinology *158*, 1217–1230. https://doi.org/10.1210/en.2016-1607.

74. Deshmukh, A.S., Peijs, L., Beaudry, J.L., Jespersen, N.Z., Nielsen, C.H., Ma, T., Brunner, A.D., Larsen, T.J., Bayarri-Olmos, R., Prabhakar, B.S., et al. (2019). Proteomics-based comparative mapping of the secretomes of human brown and white adipocytes reveals EPDR1 as a novel Batokine. Cell Metab. *30*, 963–975.e7. https://doi.org/10.1016/j.cmet.2019.10.001.

75. Hondares, E., Iglesias, R., Giralt, A., Gonzalez, F.J., Giralt, M., Mampel, T., and Villarroya, F. (2011). Thermogenic activation induces FGF21 expression and release in brown adipose tissue. J. Biol. Chem. *286*, 12983–12990. https://doi.org/10.1074/jbc.M110.215889.

76. Roh, H.C., Tsai, L.T.Y., Shao, M., Tenen, D., Shen, Y., Kumari, M., Lyubetskaya, A., Jacobs, C., Dawes, B., Gupta, R.K., et al. (2018). Warming induces significant reprogramming of beige, but not brown, adipocyte cellular identity. Cell Metab. *27*, 1121–1137.e5. https://doi.org/10.1016/j.cmet.2018.03.005.

77. Puigserver, P., Wu, Z., Park, C.W., Graves, R., Wright, M., and Spiegelman, B.M. (1998). A cold-inducible coactivator of nuclear receptors linked to adaptive thermogenesis. Cell *92*, 829–839. https://doi.org/10.1016/S0092-8674(00)81410-5.

78. Mootha, V.K., Lindgren, C.M., Eriksson, K.F., Subramanian, A., Sihag, S., Lehar, J., Puigserver, P., Carlsson, E., Ridderstråle, M., Laurila, E., et al. (2003). PGC-1alpha-responsive genes involved in oxidative phosphorylation are coordinately downregulated in human diabetes. Nat. Genet. *34*, 267–273. https://doi.org/10.1038/ng1180.

79. Subramanian, A., Tamayo, P., Mootha, V.K., Mukherjee, S., Ebert, B.L., Gillette, M.A., Paulovich, A., Pomeroy, S.L., Golub, T.R., Lander, E.S., et al. (2005). Gene set enrichment analysis: a knowledge-based approach for interpreting genome-wide expression profiles. Proc. Natl. Acad. Sci. USA *102*, 15545–15550. https://doi.org/10.1073/pnas.0506580102.

80. Liu, J., Jang, J.Y., Pirooznia, M., Liu, S., and Finkel, T. (2021). The secretome mouse provides a genetic platform to delineate tissue-specific in vivo secretion. Proc. Natl. Acad. Sci. USA *118*. e2005134118. https://doi.org/10.1073/pnas.2005134118.

81. Wei, W., Riley, N.M., Lyu, X., Bertozzi, C.R., and Long, J.Z. (2021). Protocol for cell type-specific labeling, enrichment, and proteomic profiling of plasma proteins in mice. Star Protoc. *2*, 101014. https://doi.org/10.1016/j.xpro.2021.101014.

82. Fernandez-Mejia, C. (2005). Pharmacological effects of biotin. J. Nutr. Biochem. *16*, 424–427. https://doi.org/10.1016/j.jnutbio.2005.03.018.

83. Crewe, C., Funcke, J.B., Li, S., Joffin, N., Gliniak, C.M., Ghaben, A.L., An, Y.A., Sadek, H.A., Gordillo, R., Akgul, Y., et al. (2021). Extracellular vesicle-based interorgan transport of mitochondria from energetically stressed adipocytes. Cell Metab. *33*, 1853–1868.e11. https://doi.org/10.1016/j.cmet.2021.08.002.

84. Gonzalez-Gil, A.M., and Elizondo-Montemayor, L. (2020). The role of exercise in the interplay between myokines, hepatokines, osteokines, adipokines, and modulation of inflammation for energy substrate redistribution and fat mass loss: a review. Nutrients *12*, 1899. https://doi.org/10.3390/nu12061899.

85. Ruiz-Ramie, J.J., Barber, J.L., and Sarzynski, M.A. (2019). Effects of exercise on HDL functionality. Curr. Opin. Lipidol. *30*, 16–23. https://doi.org/10.1097/MOL.0000000000000568.

86. Jörnvall, H., von Bahr-Lindström, H., and Jeffery, J. (1984). Extensive variations and basic features in the alcohol dehydrogenase-sorbitol dehydrogenase family. Eur. J. Biochem. *140*, 17–23. https://doi.org/10.1111/j.1432-1033.1984.tb08061.x.

87. El-Kabbani, O., Darmanin, C., and Chung, R.P. (2004). Sorbitol dehydrogenase: structure, function and ligand design. Curr. Med. Chem. *11*, 465–476. https://doi.org/10.2174/0929867043455927.

88. Revollo, J.R., Grimm, A.A., and Imai, S. (2004). The NAD biosynthesis pathway mediated by nicotinamide phosphoribosyltransferase regulates Sir2 activity in mammalian cells. J. Biol. Chem. *279*, 50754–50763. https://doi.org/10.1074/jbc.M408388200.

89. Garten, A., Schuster, S., Penke, M., Gorski, T., de Giorgis, T., and Kiess, W. (2015). Physiological and pathophysiological roles of NAMPT and NAD metabolism. Nat. Rev. Endocrinol. *11*, 535–546. https://doi.org/10.1038/nrendo.2015.117.

90. Revollo, J.R., Körner, A., Mills, K.F., Satoh, A., Wang, T., Garten, A., Dasgupta, B., Sasaki, Y., Wolberger, C., Townsend, R.R., et al. (2007). Nampt/PBEF/Visfatin regulates insulin secretion in beta cells as a systemic NAD biosynthetic enzyme. Cell Metab. *6*, 363–375. https://doi.org/10.1016/j.cmet.2007.09.003.

91. Körner, A., Garten, A., Blüher, M., Tauscher, R., Kratzsch, J., and Kiess, W. (2007). Molecular characteristics of serum visfatin and differential detection by immunoassays. J. Clin. Endocrinol. Metab. *92*, 4783–4791. https://doi.org/10.1210/jc.2007-1304.

92. Boström, P., Wu, J., Jedrychowski, M.P., Korde, A., Ye, L., Lo, J.C., Rasbach, K.A., Boström, E.A., Choi, J.H., Long, J.Z., et al. (2012). A PGC1-alpha-dependent myokine that drives brown-fat-like development of white fat and thermogenesis. Nature *481*, 463–468. https://doi.org/10.1038/nature10777.

93. Ruas, J.L., White, J.P., Rao, R.R., Kleiner, S., Brannan, K.T., Harrison, B.C., Greene, N.P., Wu, J., Estall, J.L., Irving, B.A., et al. (2012). A PGC-1alpha isoform induced by resistance training regulates skeletal muscle hypertrophy. Cell *151*, 1319–1331. https://doi.org/10.1016/j.cell.2012.10.050.

94. Blaszkiewicz, M., Wood, E., Koizar, S., Willows, J., Anderson, R., Tseng, Y.H., Godwin, J., and Townsend, K.L. (2020). The involvement of neuroimmune cells in adipose innervation. Mol. Med. *26*, 126. https://doi.org/10.1186/s10020-020-00254-3.

95. Matthews, V.B., Aström, M.B., Chan, M.H., Bruce, C.R., Krabbe, K.S., Prelovsek, O., Akerström, T., Yfanti, C., Broholm, C., Mortensen, O.H., et al. (2009). Brain-derived neurotrophic factor is produced by skeletal muscle cells in response to contraction and enhances fat oxidation via activation of AMP-activated protein kinase. Diabetologia *52*, 1409–1418. https://doi.org/10.1007/s00125-009-1364-1.

96. Tharyan, R.G., Annibal, A., Schiffer, I., Laboy, R., Atanassov, I., Weber, A.L., Gerisch, B., and Antebi, A. (2020). NFYB-1 regulates mitochondrial function and longevity via lysosomal prosaposin. Nat. Metab. *2*, 387–396. https://doi.org/10.1038/s42255-020-0200-2.

97. van Leent, M.M.T., Beldman, T.J., Toner, Y.C., Lameijer, M.A., Rother, N., Bekkering, S., Teunissen, A.J.P., Zhou, X., van der Meel, R., Malkus, J., et al. (2021). Prosaposin mediates inflammation in atherosclerosis. Sci. Transl. Med. *13*, eabe1433. https://doi.org/10.1126/scitranslmed.abe1433.

98. Tyanova, S., Temu, T., Sinitcyn, P., Carlson, A., Hein, M.Y., Geiger, T., Mann, M., and Cox, J. (2016). The Perseus computational platform for comprehensive analysis of (prote)omics data. Nat. Methods *13*, 731–740. https://doi.org/10.1038/nmeth.3901.

99. Springer, M.L., Rando, T.A., and Blau, H.M. (2002). Chapter 13. Gene delivery to muscle. Curr. Protoc. Hum. Genet. *Chapter*, Unit13.4. https://doi.org/10.1002/0471142905.hg1304s31.

100. Dumesic, P.A., Egan, D.F., Gut, P., Tran, M.T., Parisi, A., Chatterjee, N., Jedrychowski, M., Paschini, M., Kazak, L., Wilensky, S.E., et al. (2019). An evolutionarily conserved uORF regulates PGC1alpha and oxidative metabolism in mice, flies, and bluefin tuna. Cell Metab. *30*, 190–200.e6. https://doi.org/10.1016/j.cmet.2019.04.013.

101. Schweppe, D.K., Prasad, S., Belford, M.W., Navarrete-Perea, J., Bailey, D.J., Huguet, R., Jedrychowski, M.P., Rad, R., McAlister, G., Abbatiello, S.E., et al. (2019). Characterization and optimization of multiplexed quantitative analyses using high-field asymmetric-waveform ion mobility mass spectrometry. Anal. Chem. *91*, 4010–4016. https://doi.org/10.1021/acs.analchem.8b05399.

102. Rad, R., Li, J., Mintseris, J., O'Connell, J., Gygi, S.P., and Schweppe, D.K. (2021). Improved monoisotopic mass estimation for deeper

Please cite this article in press as: Mittenbühler et al., Isolation of extracellular fluids reveals novel secreted bioactive proteins from muscle and fat tissues, Cell Metabolism (2022), https://doi.org/10.1016/j.cmet.2022.12.014

proteome coverage. J. Proteome Res. *20*, 591–598. https://doi.org/10.1021/acs.jproteome.0c00563.

103. Elias, J.E., and Gygi, S.P. (2007). Target-decoy search strategy for increased confidence in large-scale protein identifications by mass spectrometry. Nat. Methods *4*, 207–214. https://doi.org/10.1038/nmeth1019.

104. Huttlin, E.L., Jedrychowski, M.P., Elias, J.E., Goswami, T., Rad, R., Beausoleil, S.A., Villén, J., Haas, W., Sowa, M.E., and Gygi, S.P. (2010). A tissue-specific atlas of mouse protein phosphorylation and expression. Cell *143*, 1174–1189. https://doi.org/10.1016/j.cell.2010.12.001.

105. Savitski, M.M., Wilhelm, M., Hahne, H., Kuster, B., and Bantscheff, M. (2015). A scalable approach for protein false discovery rate estimation in large proteomic data sets. Mol. Cell. Proteomics *14*, 2394–2404. https://doi.org/10.1074/mcp.M114.046995.

106. Wang, X., Spandidos, A., Wang, H., and Seed, B. (2012). PrimerBank: a PCR primer database for quantitative gene expression analysis, 2012 update. Nucleic Acids Res. *40*, D1144–D1149. https://doi.org/10.1093/nar/gkr1013.

107. Spandidos, A., Wang, X., Wang, H., and Seed, B. (2010). PrimerBank: a resource of human and mouse PCR primer pairs for gene expression detection and quantification. Nucleic Acids Res. *38*, D792–D799. https://doi.org/10.1093/nar/gkp1005.

108. Spandidos, A., Wang, X., Wang, H., Dragnev, S., Thurber, T., and Seed, B. (2008). A comprehensive collection of experimentally validated primers for polymerase chain reaction quantitation of murine transcript abundance. BMC Genomics *9*, 633. https://doi.org/10.1186/1471-2164-9-633.

109. Wang, X., and Seed, B. (2003). A PCR primer bank for quantitative gene expression analysis. Nucleic Acids Res. *31*, e154. https://doi.org/10.1093/nar/gng154.

110. Dobin, A., Davis, C.A., Schlesinger, F., Drenkow, J., Zaleski, C., Jha, S., Batut, P., Chaisson, M., and Gingeras, T.R. (2013). STAR: ultrafast universal RNA-seq aligner. Bioinformatics *29*, 15–21. https://doi.org/10.1093/bioinformatics/bts635.

111. Love, M.I., Huber, W., and Anders, S. (2014). Moderated estimation of fold change and dispersion for RNA-seq data with DESeq2. Genome Biol. *15*, 550. https://doi.org/10.1186/s13059-014-0550-8.

112. Cornwell, M., Vangala, M., Taing, L., Herbert, Z., Köster, J., Li, B., Sun, H., Li, T., Zhang, J., Qiu, X., et al. (2018). VIPER: visualization pipeline for RNA-seq, a Snakemake workflow for efficient and complete RNA-seq analysis. BMC Bioinformatics *19*, 135. https://doi.org/10.1186/s12859-018-2139-9.

Please cite this article in press as: Mittenbühler et al., Isolation of extracellular fluids reveals novel secreted bioactive proteins from muscle and fat tissues, Cell Metabolism (2022), https://doi.org/10.1016/j.cmet.2022.12.014

STAR★METHODS

KEY RESOURCES TABLE

REAGENT or RESOURCE	SOURCE	IDENTIFIER
Antibodies		
Goat Polyclonal Anti-Mouse IgG (H+L), HRP Conjugate	Promega	Cat#: W4021; RRID: AB_43083
Goat Polyclonal Anti-Rabbit IgG (H+L), HRP Conjugate	Promega	Cat#: W4011; RRID: AB_430833
Rabbit Polyclonal Anti-UCP1	Abcam	Cat#: ab10983; RRID: AB_2241462
Rabbit Polyclonal Anti-alpha-tubulin	Cell signaling	Cat#: 2144; RRID: AB_2210548
Rabbit Monoclonal Anti-GFP	Cell signaling	Cat#: 2956; RRID: AB_1196615
Mouse Monoclonal Anti-OXPHOS cocktail	Abcam	Cat#: ab110413; RRID: AB_2629281
Rabbit Monoclonal Anti-GOLGIN 97	Cell signaling	Cat#: 13192; RRID: AB_2798144
Rabbit Monoclonal Anti-LAMIN A/C	Abcam	Cat#: ab169532
Rabbit Monoclonal Anti-BCL2	Cell signaling	Cat#: 3498; RRID: AB_1903907
Bacterial and virus strains		
pAd-GFP	This paper	N/A
pAd-PGC1α	This paper	N/A
pAd-PSAP	This paper	N/A
Critical commercial assays		
R&D Systems Proteome Purify 2 Mouse Serum Protein Immunodepletion Resin	R&D Systems	Cat#: MIDR002020
IL-6 ELISA Kit	R&D Systems	Cat#: MB100B
Adeno-X Rapid Titer Kit	Takara Bio	Cat#: 632250
ViraPower Adenoviral Expression System	Invitrogen	Cat#: K4930-00
pAd/CMV/V5-DEST Gateway Vector Kit	Thermo Fisher	Cat#: V49320
TMTpro 16plex Label Reagent Set	Thermo Fisher	Cat#: A44522
Deposited data		
Proteomics data, mm01-mm06, Tables S1, S2, S3, S5, S6, and S7	This paper	ProteomeXchange: PXD031982
Proteomics data, mm07, Table S4	This paper	ProteomeXchange: PXD037731
RNAseq of pAd transduced iWAT cells	This paper	GEO: GSE216094
Data S1 – Source Data	This paper	Data S1
Experimental models: Cell lines		
HEK 293A	Invitrogen	Cat#: R70507; RRID: CVCL_6910
Experimental models: Organisms/strains		
Mouse: C57BL/6J	The Jackson Laboratory	RRID: IMSR_JAX:000664; Strain #:000664
Mouse: C57BL/6-Tg(Ckm-Ppargc1a)31Brsp/J	Lin et al.[49]	RRID: IMSR_JAX:008231; Strain #:008231
Oligonucleotides		
Psap Exon 3-5 for qPCR	IDT	Mm.PT.58.29345087
Psap Exon 5-6 for qPCR	IDT	Mm.PT.58.32763434
Primers for qPCR, see Table S8	This paper	N/A
pAd psap_attb1_forw: GGGGACAAGTTTGTACAAAAAAGCAGGCTTCaccATGGTCTGGAGCAAGCCCACAGC	This paper	N/A

(*Continued on next page*)

Please cite this article in press as: Mittenbühler et al., Isolation of extracellular fluids reveals novel secreted bioactive proteins from muscle and fat tissues, Cell Metabolism (2022), https://doi.org/10.1016/j.cmet.2022.12.014

Continued

REAGENT or RESOURCE	SOURCE	IDENTIFIER
pAd psap_attB2_rev: GGGGACCACTTTGTACAAGAAAGCTGGGTGCT AGTTCCACACATGGCGTTTGC	This paper	N/A
pAd gfp_attb1_forw: GGGGACAAGTTTGTACAA AAAAGCAGGCTgccgccATGGTGAGCAAGGGCGAGG	This paper	N/A
pAd gfp_attb1_rev: GGGGACCACTTTGTACAAG AAAGCTGGGTtCTTGTACAGCTCGTCCATGC	This paper	N/A
pAd pgc1a_attb1_forw: GGGGACAAGTTTGTACAA AAAAGCAGGCTgccgccATGGCTTGGGACATGTGCAG	This paper	N/A
pAd pgc1a_attb1_rev: GGGGACCACTTTGTACAAGAAAGCTGGGTT TACCTGCGCAAGCTTCTCT	This paper	N/A
Recombinant DNA		
cDNA PSAP	Horizon	AI037048
cDNA GFP	GenBank	AAB02576.1
cDNA PGC1α	OriGene	NM_008904.3
Software and algorithms		
GSEA 4.1.0	Mootha et al.[78]; Subramanian et al.[79]	https://www.gsea-msigdb.org/gsea/index.jsp
GOrilla	Eden et al.[38,39]	http://cbl-gorilla.cs.technion.ac.il
STRING	Szklarczyk et al.[45]	https://string-db.org
Perseus	Tyanova et al.[98]	https://maxquant.net/perseus/
Biorender	Biorender	https://biorender.com/
Others		
20 μm nylon mesh for EF isolation	Millipore Sigma	Cat#: NY2004700

RESOURCE AVAILABILITY

Lead contact

Further information and requests for resources and reagents should be directed to and will be fulfilled by the lead contact, Bruce Spiegelman (bruce_spiegelman@dfci.harvard.edu).

Materials availability

Unique material generated in this study, such as adenoviruses, will be available from the lead contact upon request.

Data and code availability

- Source data for graphs can be found in Data S1. The mass spectrometry proteomics data have been deposited to the ProteomeXchange Consortium via the PRIDE partner repository with the dataset identifier ProteomeXchange: PXD031982, PXD037731. The RNAseq data have been deposited to GEO: GSE216094.
- This paper does not report original code
- Any additional information required to reanalyze the data reported in this paper is available from the lead contact upon request.

EXPERIMENTAL MODEL AND SUBJECT DETAILS

Mice

Mice used for this study were housed at 22°C, unless stated differently. They were housed at a 12 h light/dark cycle and had unlimited access to food and water. Wild-type, 8 week old, male mice for exercise experiments and cold adaptation studies were obtained from The Jackson Laboratory (C57BL/6J, #000664). Mice were randomly assigned to control and experimental groups. Hemizygous transgenic MCK-PGC1α mice have been described previously[49] and were bred in house on a C57BL/6J background. Wild-type littermates served as controls. Transgenic MCK-PGC1α and control mice were mixed gender and 8 weeks old. All experiments were performed according to procedures approved by the Institutional Animal Care and Use Committee (IACUC) of Beth Israel Deaconess Medical Center and were in line with NIH guidelines.

Please cite this article in press as: Mittenbühler et al., Isolation of extracellular fluids reveals novel secreted bioactive proteins from muscle and fat tissues, Cell Metabolism (2022), https://doi.org/10.1016/j.cmet.2022.12.014

Cell culture

Primary myoblasts were isolated from C57BL/6J mice. Cells were maintained in growth medium DMEM/F12 supplemented with 20% fetal bovine serum and penicillin/streptomycin at 37°C. Inguinal white adipose stromal-vascular fraction (SVF) was isolated from 6-10 week old C57BL/6J mice. Cells were maintained in growth medium DMEM/F12 supplemented with 10% fetal bovine serum and penicillin/streptomycin at 37°C. For primary cell isolation protocols see "method details" section.

HEK293A cells were obtained from Invitrogen (Cat#: R70507) and maintained in growth medium DMEM supplemented with 10% fetal bovine serum and penicillin/streptomycin at 37°C.

METHOD DETAILS

Exercise protocol

Mice were trained on a motorized treadmill (Columbus Instruments) for three consecutive days. The exercise protocol was adapted from Reddy et al. with minor modifications.[36] In brief, mice were trained 5 min at 12 m/min followed by a 1 min rest. Subsequently, mice run another 5 min at 12 m/min and 5 min at 14 m/min. On the third day of training, sedentary mice were removed from the treadmill and exercise mice were kept running for a total of 45 min with ramped up speed of 2 m/min every 5 mins and maximum speed of 26 m/min. Mice were sacrificed either 0 h, 30 min, 60 min, 2 h, or 4 h after the run, as indicated. Blood samples were taken, the gastrocnemius muscle was dissected and EF was isolated. To isolate serum, blood was allowed to clot for 15 min at room temperature, and centrifuged 10 min at 10,000 g to remove the clot. To isolate plasma, blood was collected into BD Microtainer Tube, Blood Collection Lithium Heparin (BD, 365985) and centrifuged for 10 min at 10,000 g. Tissue, EF, and serum/plasma samples were snap frozen and stored at -80°C for further analysis. EF was isolated 60 min post exercise for proteomic analysis.

For the GFP-exercise experiment (Figure 2B), $1.7x10^8$ infectious particles of GFP-Adenovirus (vector generation described below) were injected into gastrocnemius muscle two weeks prior to the exercise experiment. Subsequently, mice were trained as described above. Sedentary control mouse was removed from the treadmill and the exercised mouse was kept running until exhaustion with ramped up speed as described above. EF and tissue was isolated directly after exercise.

Exposure to 4°C, 22°C, or 30°C

For long term adaptation, 8 week old wildtype male mice were exposed to either 4°C, 22°C, or 30°C for two consecutive weeks. Subsequently, blood samples were taken, adipose tissue and gastrocnemius muscle were dissected and EF was isolated. Blood was clotted for 15 min at room temperature, and centrifuged 10 min at 10,000 g to remove the clot. Tissue, EF, and serum samples were snap frozen and stored at -80°C for further analysis. For short term exposure, mice were acclimated at 30°C for 3 weeks before being shifted to 4°C. At the indicated time point (0 h, 3 h, 6 h, 12 h, 24 h), tissues from 5 mice were harvested and kept at -80°C for further processing and analysis.

Extracellular fluid isolation

EF isolation was modified from previous procedures.[32,34–36] Gastrocnemius muscle, BAT, iWAT, or eWAT was dissected, placed into a 20 μm nylon mesh (Millipore Sigma, NY2004700), and fixed in a 1.5 ml tube. Subsequently, tissue was centrifuged at 600–800 g for 10 min at 4°C. EF was snap frozen and kept at -80°C for further processing and analysis. For proteomics analysis of cold exposed adipose tissues, EF of both fat pads of 5 mice were pooled for each sample and prepared for proteomics analysis. For muscle EF proteomics analysis, EF of left and right gastrocnemius muscles of the same mouse were pooled and prepared for proteomics analysis. EF volume was measured and protein concentration was determined using Pierce BCA Protein Assay Kit (Thermo Scientific, 23227).

Immunodepletion of EF and Serum

Serum and EF samples were immunodepleted using R&D Systems Proteome Purify 2 Mouse Serum Protein Immunodepletion Resin (R&D Systems, MIDR002020). The protocol was performed as described by the manufacturer. Briefly, 10 μl EF (pooled from either left and right gastrocnemius muscle of the same mouse or from left and right fat pads of 5 mice) or serum was mixed with 1 ml of immunodepletion resin and incubated on a rotator shaker at room temperature for 45 min. Subsequently 1 ml of resin was equally split into two SpinX filter tubes (R&D Systems, SPINX8160036) and centrifuged at 1,500 g for 2 min. Flowthrough was collected, protein concentration was analyzed using Pierce Micro BCA Protein Assay Kit (Thermo Scientific, 23235), and samples were snap frozen and kept at -80°C for further analysis.

Primary myoblast isolation and culturing

Primary myoblasts were isolated from C57BL/6J mice and propagated on collagen-coated tissue culture plates (Corning) in growth medium containing an equal mixture of F10 (Thermo, 11550043) and DMEM (Corning, 10017CV) supplemented with 20% fetal bovine serum and penicillin/streptomycin.[99] One day prior to differentiation, myoblasts were plated on 10 cm collagen-coated plates at a density of $3.6x10^6$ cells per plate. The next day, differentiation was initiated by washing with PBS and then adding differentiation medium: DMEM with 5% horse serum (HyClone) and penicillin/streptomycin. One day later, differentiation medium was replaced and adenovirus encoding GFP or PGC1α was added at MOI 100. Sixteen hours later, the differentiation medium was replaced. After an additional 24 hours, the cells were washed 3X with PBS and then incubated in DMEM with 1 mM sodium pyruvate and no serum. After

Please cite this article in press as: Mittenbühler et al., Isolation of extracellular fluids reveals novel secreted bioactive proteins from muscle and fat tissues, Cell Metabolism (2022), https://doi.org/10.1016/j.cmet.2022.12.014

CellPress

8 hours of conditioning, the medium was removed and centrifuged twice at 5 min 600 g to remove insoluble material. For each replicate, approximately 50 ml conditioned medium was concentrated to 2 ml using a 3000 MWCO spin column (Amicon), then snap frozen and stored at -80°C.

Conditioned medium preparation for mass spectrometry

2 ml of concentration conditioned medium combined with an equal volume of protein lysis buffer (2% SDS, 150 mM NaCl, 50 mM HEPES pH 8.8, 5 mM TCEP, Protease Inhibitor (Sigma Aldrich, 11836170001)) and vortexed for 2 min. Samples were placed at 60°C for 30 min and subsequently cooled down to room temperature (RT) for 10 min. 14 mM iodoacetamide was added and incubated for 45 min at RT in the dark. DTT was added to a final concentration of 5 mM and incubated 15 min in the dark. Next, proteins were precipitated. Therefore, 1 volume of TCA stock (Sigma Aldrich, T0699) was added to 4 volumes of protein sample, mixed thoroughly, and placed on ice to precipitate overnight. Subsequently, samples were centrifuged at 17,000 g for 10 min at 4°C. Protein pellets were washed 4X with 1 ml of ice cold HPLC grade methanol (Fisher Scientific, A4544). Protein pellets were dried and resuspended for overnight digest using 6 μg LysC and 6 μg trypsin in 25 mM HEPES pH 8.5 and 2M urea. Samples were acidified with 10% acetic acid, clarified by centrifugation 16,000 g for 5 min, and subjected to C18 solid-phase extraction (50 mg SPE) using Sep-Pak cartridges. Isobaric labeling of peptides was performing using 10-plex tandem mass tag reagents (Thermo). 5 mg of reagents were dissolved in 252 μl acetonitrile (ACN) and 1/10 of the solution was added to 100 μg of peptides dissolved in 100 μl of 200 mM EPPS. After 1 hour (RT), the reaction was quenched by adding 3 μl of 5 % hydroxylamine. Labeled peptides were combined and acidified prior to C18 SPE on Sep-Pak cartridges (Waters, WAT054955), followed by drying in a speed-vac. Next, glycosylated peptides were separated and enzymatically deglycosylated. Briefly, peptides were resuspended in 0.1% TFA in 50% ACN; sodium periodate was added to 10 mM and sample was rotated at 4°C for 1 h, followed by C18 SPE. Peptides were subsequently bound to hydrazine resin (Thermo) overnight at RT with rotation in 50% ACN and 0.1% TFA. The hydrazine resin was washed twice with 100mM ammonium bicarbonate, resuspended in 500 μl 100 mM ammonium bicarbonate, and bound peptides were released by addition of 30 μl NEB deglycosylation mix II (P6044S) with rotation for 6 h at 37°C. Subsequently, the supernatant was brought to 60% ACN, acidified to pH 1 using TFA, and passed over C18 SPE material. Flow-through was desalted by C18 SPE and proceeded to mass spectrometry.

Muscle Tissue preparation for Mass Spectrometry

To isolate the soluble fraction from muscle tissue, 1% NP-40 lysis buffer (1% NP-40, 50 mM Tris pH 8.0, 5 mM EDTA, Phosphatase Inhibitor (Sigma Aldrich, 04906837001), Protease Inhibitor (Sigma Aldrich, 11836170001)) was added to gastrocnemius muscles and tissues were homogenized using a bead homogenizer for 20 min at max speed (Qiagen, TissueLyser II). Subsequently, homogenates were centrifuged at 17,000 g at 4°C for 10 min to pellet the muscle contractile fraction. The supernatant was transferred into a new tube and the protein concentration was determined using bicinchoninic acid assay (Fisher Scientific, 23225). Samples were snap frozen and stored at -80°C for further processing.

Protein digest and peptide isobaric labeling

50–100 μg of immunodepleted EF, immunodepleted serum, or soluble fraction of muscle lysates were mixed 1:1 with protein lysis buffer (2% SDS, 150 mM NaCl, 50 mM HEPES pH 8.8, 5 mM dithiothreitol (DTT), Phosphatase Inhibitor (Sigma Aldrich, 04906837001), Protease Inhibitor (Sigma Aldrich, 11836170001)) and vortexed for 2 min. Samples were placed at 60 °C for 30 min and subsequently cooled down to room temperature (RT) for 10 min. To reduce disulfide bonds and alkylate cysteine residues, 14 mM iodoacetamide was added and incubated for 45 min at RT in the dark. DTT was added to a final concentration of 5 mM and incubated 15 min in the dark. Next, proteins were precipitated. Therefore, 1 volume of TCA stock (Sigma Aldrich, T0699) was added to 4 volumes of protein sample, mixed thoroughly, and placed on ice to precipitate overnight. Subsequently, samples were centrifuged at 17,000 g for 10 min at 4°C. Protein pellets were washed 4x with 1 ml of ice cold HPLC grade methanol (Fisher Scientific, A4544). Protein pellets were dried and resuspended in 200 mM EPPS buffer (Fisher Scientific, J61476). For protein digestion LysC (1/100 enzyme/protein ratio) and trypsin (1/200 enzyme/protein ratio) were added and incubated overnight at 37°C. Next, samples were acidified with formic acid (FA) to a pH ~2. Peptides were labeled using 16-plex tandem mass tag (TMT) reagents (Thermo Fisher Scientific, Rockford, IL). 5.0 mg of reagents were dissolved in 252 μl acetonitrile (ACN) (Honeywell) and 1/10 of the solution was added to 100 μg of peptides dissolved in 100 μl of 200 mM EPPS. After 1 hour (RT), the reaction was quenched by adding 3 μl of 5 % hydroxylamine. Labeled peptides were combined and acidified prior to C18 SPE on Sep-Pak cartridges (Waters, WAT054955). Peptides were eluted in 70% acetonitrile, 1% formic acid and dried by vacuum centrifugation. The peptides were resuspended in 10 mM ammonium bicarbonate pH 8, 5% acetonitrile and fractionated by basic pH reverse phase HPLC. In total 24 fractions were collected. The fractions were dried in a vacuum centrifuge, resuspended in 5% acetonitrile, 1% formic acid and desalted by stage-tip. Final peptides were eluted in, 70% acetonitrile, 1% formic acid, dried, and finally resuspended in 5% acetonitrile, 5% formic acid. 12 of 24 fractions were analyzed by LC-MS/MS.

Mass spectrometry data acquisition

All data were collected on an Orbitrap Eclipse mass spectrometer (ThermoFisher Scientific) coupled to a Proxeon EASY-nLC 1000 LC pump (ThermoFisher Scientific) except the *in vitro* conditioned media, which was collected on Orbitrap Fusion Lumos as previously described.[100] Peptides were separated using a 90-min gradient at 500 nL/min on a 30-cm column (i.d. 100 μm, Accucore, 2.6 μm, 150 Å) packed inhouse. Data in Tables S1 and S2 were collected as follows: High-field asymmetric-waveform ion mobility

Please cite this article in press as: Mittenbühler et al., Isolation of extracellular fluids reveals novel secreted bioactive proteins from muscle and fat tissues, Cell Metabolism (2022), https://doi.org/10.1016/j.cmet.2022.12.014

spectroscopy (FAIMS) was enabled during data acquisition with compensation voltages (CVs) set as −40 V, −60 V, and −80 V.[101] MS1 data were collected using the Orbitrap (60,000 resolution; maximum injection time 50 ms; AGC 4×10^5). Determined charge states between 2 and 6 were required for sequencing, and a 60 s dynamic exclusion window was used. Data dependent mode was set as cycle time (1 s). MS2 scans were performed in the Orbitrap with HCD fragmentation (isolation window 0.5 Da; 50,000 resolution; NCE 36%; maximum injection time 86 ms; AGC 1×10^5). Data in Tables S3, S4, S5, S6, and S7 were collected as follows: High-field asymmetric-waveform ion mobility spectroscopy (FAIMS) was enabled during data acquisition with compensation voltages (CVs) set as −40 V.[101] MS1 data were collected using the Orbitrap (60,000 resolution; maximum injection time 50 ms; AGC 10×10^5). Determined charge states between 2 and 6 were required for sequencing, and a 60 s dynamic exclusion window was used. Data dependent mode was set as cycle time (3 s). MS2 scans were performed in the Orbitrap with HCD fragmentation (isolation window 0.5 Da; 50,000 resolution; NCE 37.5%; maximum injection time 300 ms; AGC 1×10^5).

Mass spectrometry data analysis

Raw files were first converted to mzXML, and monoisotopic peaks were re-assigned using Monocle.[102] Database searching included all mouse entries from Uniprot (downloaded in July, 2014). The database was concatenated with one composed of all protein sequences in the reversed order. Sequences of common contaminant proteins (e.g., trypsin, keratins, etc.) were appended as well. Searches were performed using the comet search algorithm. Searches were performed using a 50-ppm precursor ion tolerance and 0.02 Da product ion tolerance. TMTpro on lysine residues and peptide N termini (+304.2071 Da) and carbamidomethylation of cysteine residues (+57.0215 Da) were set as static modifications, while oxidation of methionine residues (+15.9949 Da) was set as a variable modification.

Peptide-spectrum matches (PSMs) were adjusted to a 1% false discovery rate (FDR).[103] PSM filtering was performed using linear discriminant analysis (LDA) as described previously,[104] while considering the following parameters: comet log expect, different sequence delta comet log expect (percent difference between the first hit and the next hit with a different peptide sequence), missed cleavages, peptide length, charge state, precursor mass accuracy, and fraction of ions matched. Each run was filtered separately. Protein-level FDR was subsequently estimated at a data set level. For each protein across all samples, the posterior probabilities reported by the LDA model for each peptide were multiplied to give a protein-level probability estimate. Using the Picked FDR method,[105] proteins were filtered to the target 1% FDR level.

For reporter ion quantification, a 0.003 Da window around the theoretical *m/z* of each reporter ion was scanned, and the most intense *m/z* was used. Reporter ion intensities were adjusted to correct for the isotopic impurities of the different TMTpro reagents according to manufacturer specifications. Peptides were filtered to include only those with a summed signal-to-noise (SN) of 160 or greater across all channels. For each protein, the filtered peptide TMTpro SN values were summed to generate protein quantification.

Statistical analysis MS

Statistical analysis was performed using Perseus.[98] P-values were calculated by the Student's t-test. Fold changes were calculated by averaging abundance of each group and dividing "treated" group by control group average. Q-values were calculated by a permutation-based false discovery rate estimation and proteins with q-values < 0.05 were considered statistically significant.

Gene-Ontology analysis was performed using GOrilla.[38,39] Two lists of genes (target and background sets) were used, all quantified proteins were used as background set. P-value threshold was set to $< 10^{-3}$. Enrichment (N, B, n, b) is defined as follows: N - is the total number of genes, B - is the total number of genes associated with a specific GO term, n - is the number of genes in the top of the user's input list or in the target set when appropriate, b - is the number of genes in the intersection, Enrichment = (b/n) / (B/N). Enrichment cutoff was set to 1.5. KEGG pathway analysis was performed on significantly downregulated secreted proteins in Figures 2E and S2C using String.[45] Whole mouse genome was used as background set.

IL-6 ELISA

IL-6 ELISA (R&D, MB100B) for EF and serum samples of mice, sedentary and exercised or pre- and post-exercise, was performed according to the manufactures instructions.

Gene expression analysis by qRT-PCR

Total RNA was isolated from cells and tissues using TRIzol reagent (Invitrogen, 15596018) and RNeasy Mini purification kit (Qiagen, 74104) according the manufactures protocol. Tissues were homogenized in TRIzol reagent using a bead homogenizer for 20 min at max speed (Qiagen, TissueLyser II). DNA was digested on column using RNase-Free DNase Set (Qiagen, 79254). RNA was reversely transcribed using High-Capacity cDNA Reverse Transcription kit with RNase Inhibitor (Applied Biosystems, 4374966) and gene expression was determined by quantitative PCR (QuantStudio™ 6 Pro Real-Time PCR System, 384-well). Briefly, cDNA was mixed with 250-500 nmol primers and GoTaq qPCR System (Promega, A6002). Relative mRNA levels of the gene of interests were normalized to mRNA level of *Rplp0*. If not stated otherwise, primer sequences were chosen from PrimerBank.[106–109] Used primers and sequences are listed in Table S8.

Primary adipocyte isolation and cell culture

Inguinal white adipose stromal-vascular fraction (SVF) was isolated from 6-10 week old wild-type mice. In detail, iWAT was dissected, washed with ice-cold HBSS, and minced. Subsequently, suspension was incubated in HBSS (Life Technologies, 14025-092)

Please cite this article in press as: Mittenbühler et al., Isolation of extracellular fluids reveals novel secreted bioactive proteins from muscle and fat tissues, Cell Metabolism (2022), https://doi.org/10.1016/j.cmet.2022.12.014

containing 10 mg/ml collagenase D (Sigma Aldrich, 11088882001), 3 U/ml dispase II (Roche Diagnostics, 4942078001), and 10 mM CaCl2 for 30 min at 37°C with occasional shaking. To stop collagenase reaction, complete adipocyte culturing medium (DMEM/F-12 GlutaMAX (Life Technologies, 10565042), 10 % fetal bovine serum (BenchMark,100-106), 1X PenStrep (Life Technologies, 15140122), 100 μg/ml Primocin (Fisher Scientific, NC9141851)) was added to the suspension and filtered through a 100 μm cell strainer. Next, cell suspension was centrifuged at 600 g for 5 min, and SVF pellet was resuspended in complete adipocyte culturing medium, filtered through a 40 μm cell strainer and centrifuged at 600 g for 5 min. SVF pellet was resuspended and plated in complete adipocyte culturing medium. Cells were split two times at a 1:3 ratio when confluency reached 70%. For experiments, cells were grown until confluency. Afterwards, differentiation of pre-adipocytes was induced by treatment with an adipogenic cocktail (1 μM rosiglitazone (Cayman Chemical, 71740), 0.5 mM 3-Isobutyl-1-methylxanthine (IBMX) (Sigma Aldrich, I5879), 1 μM dexamethasone (Sigma Aldrich, D4902), 870 nM insulin (Sigma Aldrich, I5500)) in complete adipocyte culture medium for 2 days. Subsequently, medium was changed to complete adipocyte maintenance medium containing 1 μM rosiglitazone and 870 nM insulin. Cells were fully differentiated at day 8 after induction. Adenoviral transductions were performed at day 3-4 after differentiation initiation at an MOI of 100 and cells were harvested 72h post transduction.

Recombinant adenovirus preparation

pAd-DEST expression clones were prepared using Gateway recombination cloning technology (Invitrogen, 12536-017). Primers for all constructs can be found in the key resources table. For pAd PSAP, the open reading frame (ORF) of mouse Psap was amplified from a cDNA clone (Horizon, AI037048). For pAd GFP the eGFP ORF was used (Genbank sequence ID: AAB02576.1). For pAd PGC1α the PGC1α1 ORF was use (OriGene, NM_008904.3). ORFs were inserted into pDONR221 vector via BP recombination reaction, and subcloned into pAd/CMV/V5-DEST vector via LR recombination reaction.

Adenovirus was produced using ViraPower Adenoviral Expression System (Invitrogen, K4930-00). Briefly, pAd-DEST vectors were linearized by Pac I restriction enzyme (New England Biolabs, R0547), HEK 293A cells (Invitrogen, R70507) were transfected with linearized vectors using Lipofectamine 2000 (Invitrogen, 11668500). HEK 293A cells were grown until cytopathic effect reached around 80% (10-13 days) and subsequently harvested. The viral titer was determined using Adeno-X Rapid Titer Kit (Takara Bio, 632250).

Recombinant adenovirus transduction

Adenoviral transduction was performed at day 3-4 post differentiation initiation at an multiplicity of infection (MOI) of 100 per cell. Medium was changed 24 h afterwards and cells were harvested 72 h post transduction.

Protein isolation

Tissue and cells were homogenized in RIPA buffer (50 mM Tris pH 7.4, 150 mM NaCl, 1% Triton X-100, 0.5% Sodium-Deoxycholate, 0.1% SDS, 1mM EDTA, Phosphatase Inhibitor (Sigma Aldrich, 04906837001), Protease Inhibitor (Sigma Aldrich, 11836170001)). Tissue homogenization was performed using a bead homogenizer (Qiagen, TissueLyser II). Cells were homogenized by passing suspension through a 25 gauge syringe. Subsequently, tissue and cell lysates were centrifuged at 17,000 g for 30 min, pellet was discarded and protein concentration was determined using bicinchoninic acid assay (Fisher Scientific, 23225). Samples were snap frozen and stored at -80°C for further analysis.

SDS-PAGE, Silver Stain, and Western Blot

Samples were denatured in SDS sample buffer (6X) (0.375 M Tris pH 6.8, 12 % SDS, 60 % glycerol, 0.6 M DTT, 0.06 % bromophenol blue) for 5 min at 95°C. 10-20 μg of protein was resolved on a 4-12% NuPAGE BisTris SDS–PAGE (Invitrogen) with MOPS SDS Running Buffer (Sigma Aldrich, M1254).

SDS-PAGE used for silver staining (Life Technologies, 24612) were processed according to the manufactures protocol, respectively.

For western blot, SDS-PAGE was transferred to a polyvinylidene difluoride (PVDF) membrane (Millipore, IPVH00010) using Towbin transfer buffer (25 mM Tris, 192 mM glycine, 20% (v/v) methanol). To control for correct loading and transfer, Ponceau staining was performed according to manufactures instructions (Sigma Aldrich, P7170). Membranes were blocked in 5% BSA or 5% milk in TBS containing 0.05% Tween (TBST) and incubated overnight at 4°C with primary antibody. Secondary HRP-conjugated antibodies were used, membranes were incubated in Immobilon Crescendo Western HRP substrate (Fisher Scientific, WBLUR0500), and imaged (GE Amersham Imager AI680). Used antibodies are displayed in the key resources table.

Mitochondrial respiration

Mitochondrial respiration was determined using the XF24 Extracellular Flux Analyzer (Seahorse Bioscience). Differentiated primary inguinal adipocytes were counted and equal amounts were plated per well of a seahorse plate and incubated at 37°C and 5% CO_2 overnight. Norepinephrine-stimulated respiration was induced with 500nM Norepinephrine. Uncoupled and maximal OCR was determined using oligomycin (5μM) and FCCP (5μM). Rotenone and antimycin A (5μM each) were used to inhibit complex 1- and complex 3-dependent respiration.

Please cite this article in press as: Mittenbühler et al., Isolation of extracellular fluids reveals novel secreted bioactive proteins from muscle and fat tissues, Cell Metabolism (2022), https://doi.org/10.1016/j.cmet.2022.12.014

RNA sequencing

Library preparation and sequencing

Libraries were prepared using Roche Kapa mRNA HyperPrep strand specific sample preparation kits from 200ng of purified total RNA according to the manufacturer's protocol on a Beckman Coulter Biomek i7. The finished dsDNA libraries were quantified by Qubit fluorometer and Agilent TapeStation 4200. Uniquely dual indexed libraries were pooled in an equimolar ratio and shallowly sequenced on an Illumina MiSeq to further evaluate library quality and pool balance. The final pool was sequenced on an Illumina NovaSeq 6000 targeting 40 million 150bp read pairs per library at the Dana-Farber Cancer Institute Molecular Biology Core Facilities.

RNAseq Analysis

Sequenced reads were aligned to the UCSC mm10 reference genome assembly and gene counts were quantified using STAR (v2.7.3a).[110] Differential gene expression testing was performed by DESeq2 (v1.22.1).[111] RNAseq analysis was performed using the VIPER snakemake pipeline.[112] GSEA analysis was performed to search for enriched gene sets.[78,79] For GSEA analysis, TPM cut-off was set to > 5.

QUANTIFICATION AND STATISTICAL ANALYSIS

Data are displayed as means ± S.E.M. P-values were calculated using either two-tailed Student's t-test, multiple unpaired t-tests, one-way ANOVA, and two-way ANOVA. All used statistical tests and n numbers are presented in figure legends. For cellular assays, n corresponds to the number of experimental replicates (e.g., independent transfections). For animal assays or tissue extracted from animals, n corresponds to the number of mice used per genotype or condition. Sample sizes were determined on the basis of previous experiments using similar methodologies. No statistical method was used to predetermine sample size. For exercise and cold exposure studies, mice were randomly assigned to groups. For mass spectrometry analyses, samples were processed in random order and the experimentalists were blinded to experimental conditions.

Figures have been generated using GraphPad Prism9, Adobe Illustrator, and BioRender.com.

Cell Metabolism, Volume *35*

Supplemental information

Isolation of extracellular fluids reveals novel secreted bioactive proteins from muscle and fat tissues

Melanie J. Mittenbühler, Mark P. Jedrychowski, Jonathan G. Van Vranken, Hans-Georg Sprenger, Sarah Wilensky, Phillip A. Dumesic, Yizhi Sun, Andrea Tartaglia, Dina Bogoslavski, Mu A, Haopeng Xiao, Katherine A. Blackmore, Anita Reddy, Steven P. Gygi, Edward T. Chouchani, and Bruce M. Spiegelman

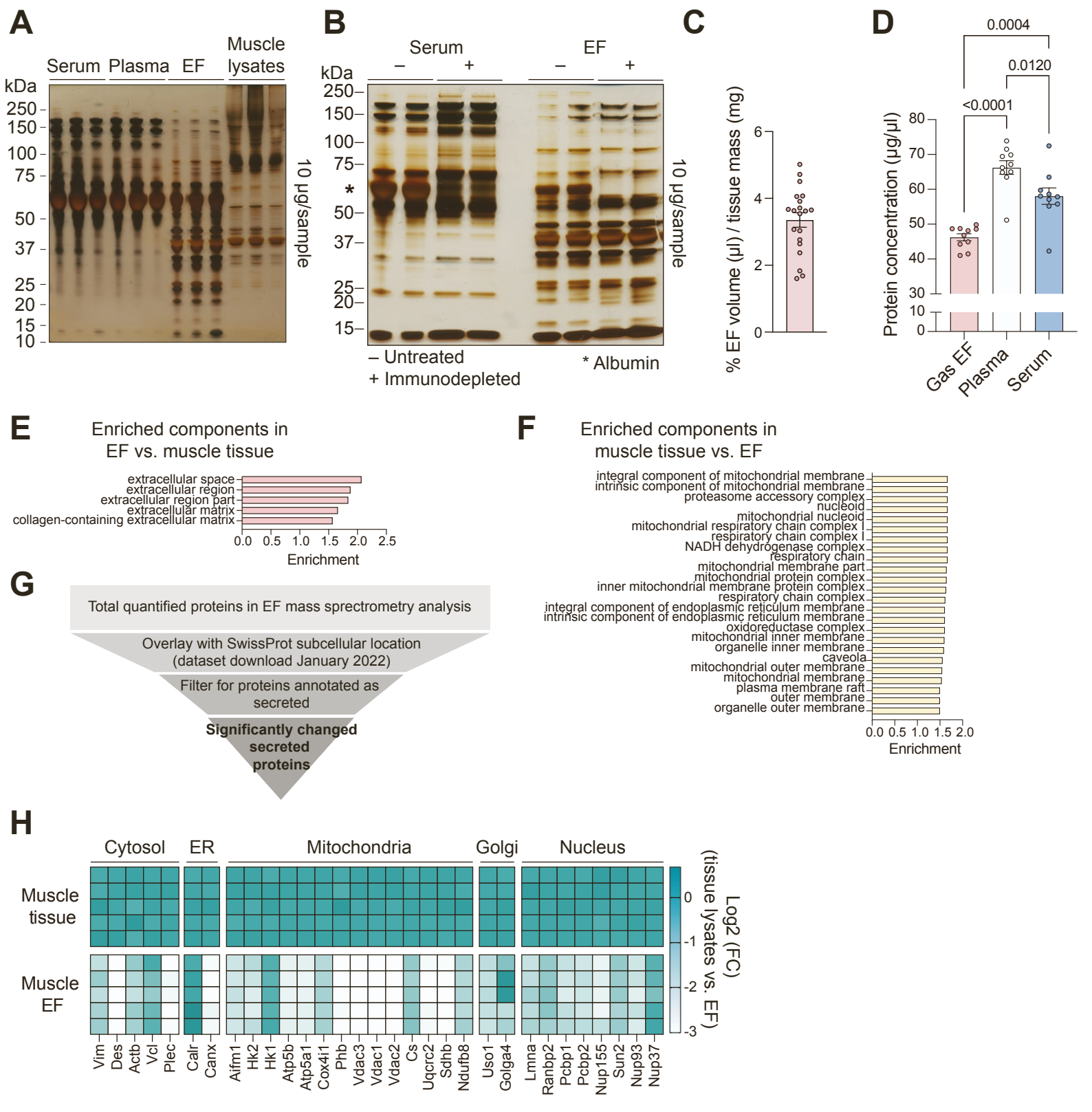
A
Serum
Plasma
EF
Muscle lysates
kDa
250
150
100
75
50
37
25
20
15
10
B
Serum
EF
kDa
250
150
100
75
*
50
37
25
20
15
10 µg/sample
10 µg/sample
– Untreated
+ Immunodepleted
* Albumin
C
% EF volume (µl) / tissue mass (mg)
D
0.0004
0.0120
<0.0001
Protein concentration (µg/µl)
Gas EF
Plasma
Serum
E
Enriched components in EF vs. muscle tissue
extracellular space
extracellular region
extracellular region part
extracellular matrix
collagen-containing extracellular matrix
Enrichment
F
Enriched components in muscle tissue vs. EF
integral component of mitochondrial membrane
intrinsic component of mitochondrial membrane
proteasome accessory complex
nucleoid
mitochondrial nucleoid
mitochondrial respiratory chain complex I
respiratory chain complex I
NADH dehydrogenase complex
respiratory chain
mitochondrial membrane part
mitochondrial protein complex
inner mitochondrial membrane protein complex
respiratory chain complex
integral component of endoplasmic reticulum membrane
intrinsic component of endoplasmic reticulum membrane
oxidoreductase complex
mitochondrial inner membrane
organelle inner membrane
caveola
mitochondrial outer membrane
mitochondrial membrane
plasma membrane raft
outer membrane
organelle outer membrane
Enrichment
G
Total quantified proteins in EF mass sprectrometry analysis
Overlay with SwissProt subcellular location (dataset download January 2022)
Filter for proteins annotated as secreted
Significantly changed secreted proteins
H
Cytosol
ER
Mitochondria
Golgi
Nucleus
Muscle tissue
Muscle EF
Log2 (FC) (tissue lysates vs. EF)
Vim
Des
Actb
Vcl
Plec
Calr
Canx
Aifm1
Hk2
Hk1
Atp5b
Atp5a1
Cox4i1
Phb
Vdac3
Vdac1
Vdac2
Cs
Uqcrc2
Sdhb
Ndufb8
Uso1
Golga4
Lmna
Ranbp2
Pcbp1
Pcbp2
Nup155
Sun2
Nup93
Nup37

Figure S1

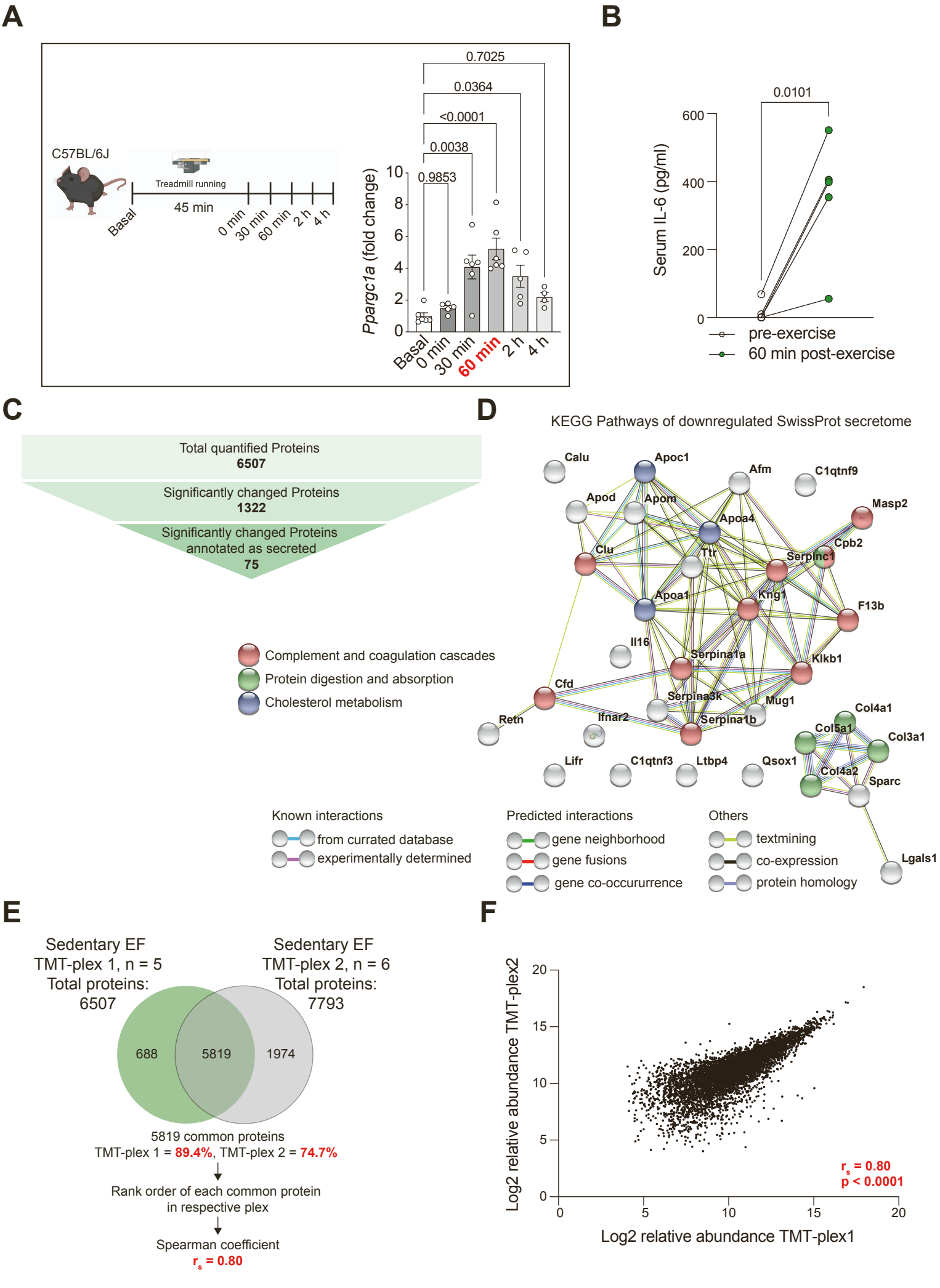
A
C57BL/6J
Treadmill running
45 min
Basal
0 min
30 min
60 min
2 h
4 h
Ppargc1a (fold change)
0.7025
0.0364
<0.0001
0.0038
0.9853
B
Serum IL-6 (pg/ml)
0.0101
pre-exercise
60 min post-exercise
C
Total quantified Proteins
6507
Significantly changed Proteins
1322
Significantly changed Proteins annotated as secreted
75
Complement and coagulation cascades
Protein digestion and absorption
Cholesterol metabolism
D
KEGG Pathways of downregulated SwissProt secretome
Calu
Apoc1
Afm
C1qtnf9
Apod
Apom
Masp2
Apoa4
Cpb2
Clu
Ttr
Serpinc1
Apoa1
Kng1
F13b
Il16
Serpina1a
Klkb1
Cfd
Serpina3k
Mug1
Retn
Ifnar2
Serpina1b
Col4a1
Col5a1
Col3a1
Lifr
C1qtnf3
Ltbp4
Qsox1
Col4a2
Sparc
Lgals1
Known interactions
from currated database
experimentally determined
Predicted interactions
gene neighborhood
gene fusions
gene co-occurrence
Others
textmining
co-expression
protein homology
E
Sedentary EF
TMT-plex 1, n = 5
Total proteins:
6507
Sedentary EF
TMT-plex 2, n = 6
Total proteins:
7793
688
5819
1974
5819 common proteins
TMT-plex 1 = 89.4%, TMT-plex 2 = 74.7%
Rank order of each common protein in respective plex
Spearman coefficient
r_s = 0.80
F
Log2 relative abundance TMT-plex2
Log2 relative abundance TMT-plex1
r_s = 0.80
p < 0.0001

Figure S2

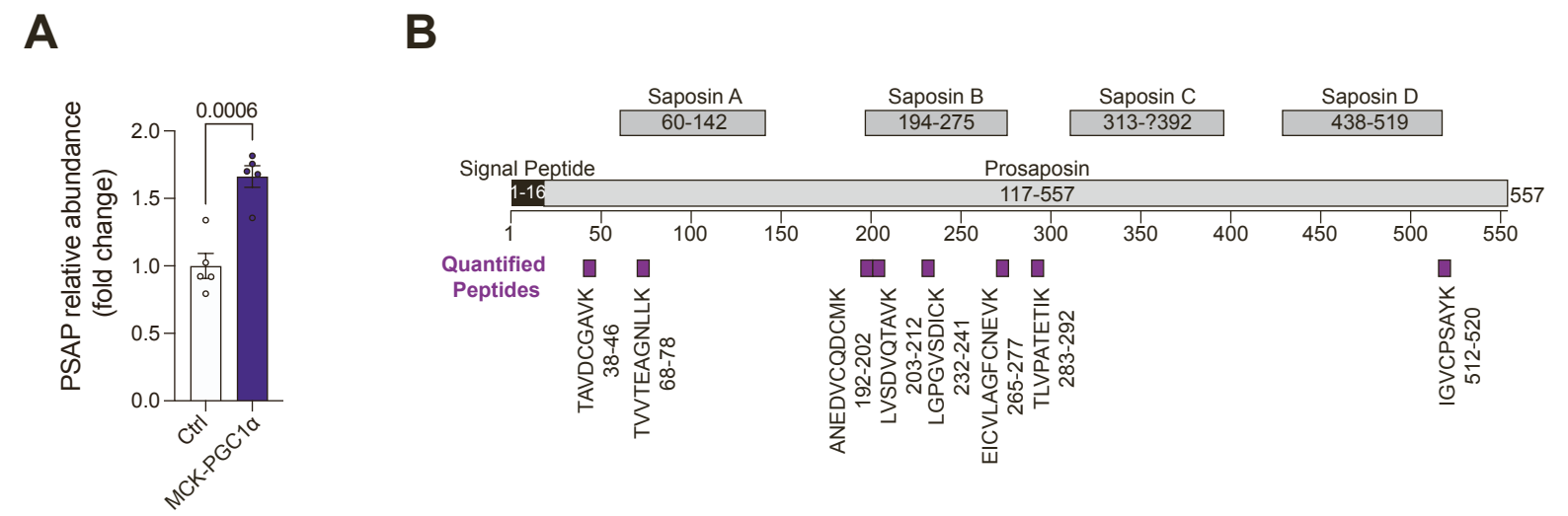
A
B
0.0006
PSAP relative abundance
(fold change)
2.0
1.5
1.0
0.5
0.0
Ctrl
MCK-PGC1α
Saposin A
60-142
Saposin B
194-275
Saposin C
313-?392
Saposin D
438-519
Signal Peptide
1-16
Prosaposin
117-557
557
1
50
100
150
200
250
300
350
400
450
500
550
Quantified
Peptides
TAVDCGAVK
38-46
TVVTEAGNLLK
68-78
ANEDVCQDCMK
192-202
LVSDVQTAVK
203-212
LGPGVSDICK
232-241
EICVLAGFCNEVK
265-277
TLVPATETIK
283-292
IGVCPSAYK
512-520

Figure S3

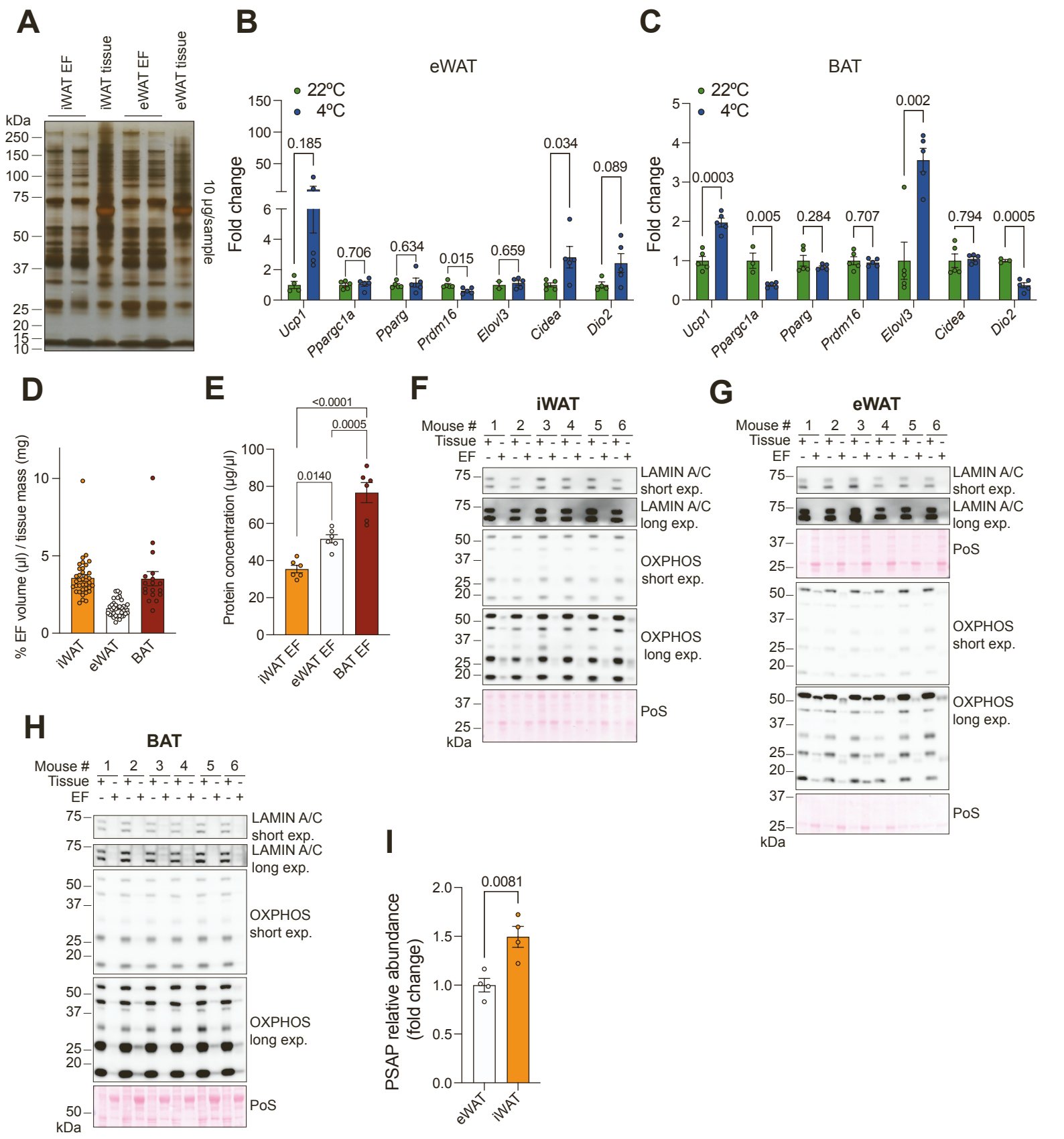
A
iWAT EF
iWAT tissue
eWAT EF
eWAT tissue
kDa
250
150
100
75
50
37
25
20
15
10
10 µg/sample
B
eWAT
22ºC
4ºC
Fold change
0.185
0.706
0.634
0.015
0.659
0.034
0.089
Ucp1
Ppargc1a
Pparg
Prdm16
Elovl3
Cidea
Dio2
C
BAT
22ºC
4ºC
Fold change
0.0003
0.005
0.284
0.707
0.002
0.794
0.0005
Ucp1
Ppargc1a
Pparg
Prdm16
Elovl3
Cidea
Dio2
D
% EF volume (µl) / tissue mass (mg)
iWAT
eWAT
BAT
E
Protein concentration (µg/µl)
<0.0001
0.0005
0.0140
iWAT EF
eWAT EF
BAT EF
F
iWAT
Mouse # 1 2 3 4 5 6
Tissue + - + - + - + - + - + -
EF - + - + - + - + - + - +
LAMIN A/C short exp.
LAMIN A/C long exp.
OXPHOS short exp.
OXPHOS long exp.
PoS
kDa
G
eWAT
Mouse # 1 2 3 4 5 6
Tissue + - + - + - + - + - + -
EF - + - + - + - + - + - +
LAMIN A/C short exp.
LAMIN A/C long exp.
PoS
OXPHOS short exp.
OXPHOS long exp.
PoS
kDa
H
BAT
Mouse # 1 2 3 4 5 6
Tissue + - + - + - + - + - + -
EF - + - + - + - + - + - +
LAMIN A/C short exp.
LAMIN A/C long exp.
OXPHOS short exp.
OXPHOS long exp.
PoS
kDa
I
PSAP relative abundance (fold change)
0.0081
eWAT
iWAT

Figure S4

Supplemental Figures and Legends:

Figure S1: Experimental validation of muscle extracellular fluid protein composition. Related to Figure 1.
(A) Protein gel and subsequent silver staining of serum, plasma, EF, and muscle lysates (10 µg protein per sample).
(B) Protein gel and subsequent silver staining of immunodepleted serum and EF samples (10 µg protein per sample). – = untreated, + = immunodepleted, * = albumin.
(C) Percent EF volume (µl) to gastrocnemius tissue mass (mg) (n = 20).
(D) Protein concentration of gastrocnemius EF, plasma, and serum samples (one-way ANOVA, n = 10).
(E) GO-term component analysis of proteins higher (q-value < 0.05) in EF vs. muscle tissue (GOrilla, enrichment cut off > 1.5 [1,2]). Target set: proteins higher (q-value < 0.05) in EF vs. muscle tissue, background set: all proteins quantified by MS in this experiment (n = 5 per compartment).
(F) GO-term component analysis of proteins higher (q-value < 0.05) in muscle tissue vs. EF (GOrilla, enrichment cut off > 1.5 [1,2]). Target set: proteins higher (q-value < 0.05) in muscle tissue vs. EF, background set: all proteins quantified by MS in this experiment (n = 5 per compartment).
(G) Scheme of filtering procedure of quantified proteins.
(H) Heat map depicting fold changes of common intracellular marker proteins in muscle tissue and EF (n = 5 per compartment). Normalized to muscle tissue.
Data are means ± S.E.M.

Figure S2: Muscle extracellular fluid composition in exercise. Related to Figure 2.
(A) qRT-PCR of *Ppargc1a* gene expression normalized to *rplp0* at different timepoints after an acute bout of exercise (one-way ANOVA, n = 4-6 per timepoint).
(B) ELISA of serum IL-6 levels pre- and 60 min post-exercise, measured in the same mouse (two-tailed paired t-test, n = 5).
(C) Scheme of data filtering procedure.
(D) String analysis of KEGG-Pathways enriched among proteins significantly decreased in EF of exercised mice [3].
(E) Venn diagram of two independent prepared TMT-plexes showing overlap of quantified proteins and spearman coefficient of rank-ordered common proteins.
(F) Log2 relative abundances of all proteins commonly quantified in TMT-plex 1 and TMT-plex 2, r_s = spearman coefficient.
Data are means ± S.E.M.

Figure S3: Prosaposin in muscle extracellular fluid. Related to Figure 3.
(A) PSAP fold change of relative abundances in MCK-PGC1α vs. ctrl EF MS (two-tailed unpaired t-test, n = 5 per genotype).
(B) Scheme of *Psap* gene and quantified peptides in MS analysis.
Data are means ± S.E.M.

Figure S4: Experimental validation of fat extracellular fluid protein composition. Related to Figure 4.

(A) Protein gel and silver stain of EF and tissue lysates of iWAT and eWAT after immunodepletion.

(B) qRT-PCR of thermogenic gene expression normalized to *rplp0* in eWAT after 2 weeks room temperature or cold exposure (unpaired t-test, n = 2-5)

(C) qRT-PCR of thermogenic gene expression normalized to *rplp0* in BAT after 2 weeks room temperature or cold exposure (unpaired t-test, n = 3-5).

(D) Percent of muscle EF volume (µl) to respective adipose tissue mass (mg) of 2 weeks cold exposed mice (iWAT and eWAT n = 36, BAT n = 18).

(E) Protein concentration of respective adipose EF samples of 2 weeks cold exposed mice (one-way ANOVA, n = 6).

(F) Western blot for intracellular markers LAMIN A/C and OXPHOS proteins of iWAT EF and tissue lysates of 2 weeks cold exposed mice.

(G) Western blot for intracellular markers LAMIN A/C and OXPHOS proteins of eWAT EF and tissue lysates of 2 weeks cold exposed mice.

(H) Western blot for intracellular markers LAMIN A/C and OXPHOS proteins of BAT EF and tissue lysates of 2 weeks cold exposed mice.

(I) PSAP fold change of relative abundances in iWAT vs. eWAT EF MS (two-tailed unpaired t-test, n = 4).

Data are means ± S.E.M.

References

1. Eden, E., Lipson, D., Yogev, S., and Yakhini, Z. (2007). Discovering motifs in ranked lists of DNA sequences. PLoS Comput Biol *3*, e39. 10.1371/journal.pcbi.0030039.
2. Eden, E., Navon, R., Steinfeld, I., Lipson, D., and Yakhini, Z. (2009). GOrilla: a tool for discovery and visualization of enriched GO terms in ranked gene lists. BMC Bioinformatics *10*, 48. 10.1186/1471-2105-10-48.
3. Szklarczyk, D., Franceschini, A., Wyder, S., Forslund, K., Heller, D., Huerta-Cepas, J., Simonovic, M., Roth, A., Santos, A., Tsafou, K.P., et al. (2015). STRING v10: protein-protein interaction networks, integrated over the tree of life. Nucleic Acids Res *43*, D447-452. 10.1093/nar/gku1003.